The CLAS12 Central Neutron Detector

P. Chatagnon, J. Bettane, M. Hoballah, G. Hull, M. Imre, D. Marchand, B. Mathon, G. Murdoch, P. Naidoo, S. Niccolai, et al.

Elsevier Editorial System(tm) for NIMA Proceedings

Manuscript Draft

Manuscript Number:

Title: The CLAS12 Central Neutron Detector

Article Type: VSI: The CLAS12 Spectrometer

Keywords: Neutron detector; Plastic scintillator; Light collection; Time resolution; Time-of-flight; CLAS12

Corresponding Author: Mr. Pierre Chatagnon,

Corresponding Author's Institution:

First Author: Pierre Chatagnon

Order of Authors: Pierre Chatagnon; Julien Bettane; Mostafa Hoballah; Giulia Hull; Miktat Imre; Dominique Marchand; Bernard Mathon; Gavin Murdoch; Paul Naidoo; Silvia Niccolai; Katheryne Price; Daria Sokhan; Rong Wang

Abstract: The Central Neutron Detector is a scintillator barrel that was designed to detect 0.2-1 GeV neutrons at lab polar angles from 40° to 120° in the CLAS12 spectrometer in Hall~B at Jefferson Laboratory. The design is based on three radial layers of paddles read out at the upstream end of the barrel by photomultipliers tubes. Neighboring paddles in each layer are coupled together at the downstream end of the barrel by "U-turn" light guides. The components of this detector are presented and the performance of the detector with the first beam data taken by CLAS12 is reported.

Dear NIM editors,

The attached manuscript is entitled "The CLAS12 Central Neutron Detector" with lead author Pierre Chatagnon of IPN Orsay. This manuscript is intended to be part of the CLAS12 Spectrometer special NIM issue.

Sincerely,
Pierre Chatagnon

The CLAS12 Central Neutron Detector

P. Chatagnon[a], J. Bettane[a], M. Hoballah[a], G. Hull[a], M. Imre[a], D. Marchand[a], B. Mathon[a], G. Murdoch[b], P. Naidoo[b], S. Niccolai[a], K. Price[a], D. Sokhan[b], R. Wang[a]

[a] *Institut de Physique Nucléaire, CNRS-IN2P3, Univ. Paris-Sud, Université Paris-Saclay, 91406 Orsay Cedex, France*
[b] *University of Glasgow, Glasgow G12 8QQ, United Kingdom*

Abstract

The Central Neutron Detector is a scintillator barrel that was designed to detect 0.2-1 GeV neutrons at lab polar angles from 40° to 120° in the CLAS12 spectrometer in Hall B at Jefferson Laboratory. The design is based on three radial layers of paddles read out at the upstream end of the barrel by photomultipliers tubes. Neighboring paddles in each layer are coupled together at the downstream end of the barrel by "U-turn" light guides. The components of this detector are presented and the performance of the detector with the first beam data taken by CLAS12 is reported.

Keywords: Neutron detector, Plastic scintillator, Light collection, Time resolution, Time-of-flight, CLAS12

1. Overview

The Central Neutron Detector (CND) is the outermost of the subsystems composing the Central Detector of CLAS12 [1]. It consists of a barrel of three layers of scintillators coupled at their downstream ends with U-turn light guides and read out at their upstream ends by photomultiplier tubes (PMTs) connected to the bars via 1-m-long bent light guides to position them in a fringe-field region of the CLAS12 5-T superconducting solenoid. The CND was installed in the CLAS12 solenoid, and subsequently started its data taking, in the fall of 2017. Geant4-based simulations, calibrated with measurements carried out with the CND using cosmic rays muons, showed that the efficiencies obtainable with this detector and its photon-rejection capabilities are sufficient to collect good statistics on the beam-spin asymmetry for the neutron-DVCS reaction over a wide phase space, using the allocated beam time for CLAS12 with a deuterium target [2]. The first beam data collected by CLAS12 on a proton target confirmed the design performance. This detector will also be used in other n-DVCS experiments [3], and whenever the detection of the recoil neutron may be required (N^* program, for instance, or for all the deeply-virtual meson production reactions on the neutron).

2. Requirements

Measuring Deeply Virtual Compton Scattering (DVCS) on a neutron target ($en \rightarrow e'n'\gamma$) is one of the necessary steps to complete our understanding of the structure of the nucleon in terms of Generalized Parton Distributions (GPDs) [4, 5, 6]. DVCS on a neutron target allows one to perform a quark-flavor decomposition of the GPDs when combined with the results for DVCS on a proton target. Moreover, it plays a complementary role to DVCS on a transversely polarized proton target in the determination of the GPD E, the least known and least constrained GPD that enters Ji's sum rule [5], which links integrals of GPDs to the total angular momentum of the quarks. To measure n-DVCS on a deuterium target ($ed \rightarrow e'n\gamma(p)$) with CLAS12, the electron and the DVCS photon, emitted mainly at small angles, can be detected in the CLAS12 forward calorimeters (ECAL [7] and FT [8]), while the neutron is emitted predominantly (for ~80% of the events) at $\theta > 40°$ in the laboratory frame, with an average momentum around 0.5 GeV. These kinematic constraint conditions drive the design specifications for the CND. With the aid of the CLAS12 fast Monte Carlo tool (FASTMC), the requirements in terms of angular and momentum resolutions on the detected neutrons were determined by studying the missing mass (MM) of the $e'n'\gamma$ system. Using realistic resolutions on the electron and photon calculated by FASTMC, it was found that if the neutron momentum resolution is kept below 10%, its effect on the MM resolution is negligible with respect to the other particles in the reaction [9].

Therefore, considering that the detection capabilities of CLAS12 for electrons and high-energy photons are

fixed, the requirements of the CND are:

- good neutron identification capabilities for the kinematic range of interest ($0.2 < p_n < 1.2$ GeV, $40° < \theta_n < 80°$);
- neutron momentum resolution σ_p/p within 10%.

2.1. Constraints

The available radial space in the CLAS12 Central Detector is limited by the presence of the Central Time-of-Flight system (CTOF) [10] and of the solenoid magnet [11], which left about 10 cm free. However, the 3-cm-thick CTOF counters can also be used to detect neutrons, adding an additional 2-3% of detection efficiency. The Central Vertex Tracker (CVT) [12, 13] can be used as a veto for charged particles. Finally, the strong fringe field of the 5-T magnetic field required careful consideration for the positioning and the type of the CND PMTs.

After extensive Geant4 simulations and R&D studies devoted to examine the various options for the CND and its possible photodetectors [9], the final design choice was a barrel of standard plastic scintillator bars of trapezoidal cross section, all with their long sides parallel to the beam direction. This geometry is similar to that of the CTOF [10].

As previously stated, one of the two requirements of the CND is good neutron identification capabilities. If the charged particles are vetoed by the central tracker, the only particles remaining from the target that can be misidentified for neutrons are photons. Using plastic scintillators, the most straightforward way to distinguish neutrons from photons is by measuring their time-of-flight (TOF) and comparing the values of β:

$$\beta = \frac{P_L}{TOF \cdot c}, \tag{1}$$

where c is the speed of light and P_L is flight path of the particle from the target to the scintillator bar. This can be obtained, in our geometry, as

$$P_L = \sqrt{z^2 + r^2}, \tag{2}$$

where z and r are the hit position along the beam z axis and in the radial direction, respectively. To obtain z one must measure the time of the hit at both ends of the scintillator bar:

$$z = \frac{1}{2} \cdot v_{\text{eff}} \cdot (t_{\text{L}} - t_{\text{R}}), \tag{3}$$

where v_{eff} is the effective velocity of light propagation in the scintillator material. To know r it is necessary to have reasonably small radial segmentation: r will be given by the distance between the target and the middle of the hit paddle.

Geant4-based simulations show that to ensure a good photon/neutron separation for the neutron momentum range of the n-DVCS reaction, the CND has to be equipped with photodetectors ensuring a time resolution of about 150 ps.

3. Design

The design of the CND is a barrel, coaxial with the beamline, made of trapezoidal scintillator bars, read out via standard PMTs attached to long acrylic light guides. In order to optimize the light collection by matching the scintillator surface and the PMT entrance window, the detector is divided into 48 azimuthal segments and 3 radial layers, for a total of 24 blocks[1], 144 scintillator bars, 144 PMTs, and 72 U-turn light guides (see Fig. 1). The radial thickness of all scintillators is 30 mm. The other dimensions are listed in Table 1.

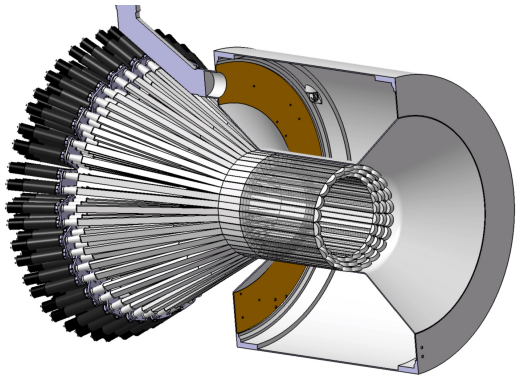

Figure 1: Drawing of the CND inserted in the CLAS12 solenoid, which is shown in a cut-view.

Layer	Inner face width (mm)	Outer face width (mm)	Length (mm)
1	35.92	39.87	665.72
2	40.0	43.95	700.0
3	44.08	48.03	734.28

Table 1: Dimensions (mm) of the trapezoidal scintillator bars of the CND. The layer numbers go from the innermost (1) to the outermost (3). The thickness of all bars is 30 mm.

[1] A "block" or "sector" is formed by three radial layers of coupled pairs of scintillator bars.

4. Hardware Components and Construction

Comparative measurements were carried out to choose the elements composing the CND. The tests were geared towards optimizing the time resolution, which is the key parameter to ensure n/γ separation, and containing all associated costs. Different prototypes were constructed and employed for measurements of time resolution and light-yield during cosmic ray testing to optimize the final design choices for scintillator type, PMT, wrapping material, PMT magnetic shielding configuration, shape of the U-turn light guide, and glue for the optical coupling. The outcomes of these tests are discussed in detail in Ref. [9]. The chosen components are:

- 144 EJ-200 scintillator bars, by Eljen Technology;
- 144 Hamamatsu R10533 2-in PMTs;
- 72 semi-circular-shaped U-turn light guides of Polymethyl Methacrylate (PMMA);
- aluminum foil as reflector material wrapping the scintillator bars;
- a 1-mm-thick mu-metal cylinder plus a 5-mm-thick mild steel cylinder to shield each PMT from the stray magnetic field of the CLAS12 solenoid;
- coupling with optical grease between PMT and light guide;
- M-Bond200 glue for the junctions between scintillators and light guides.

The 24 blocks composing the CND were assembled in the mechanical shop of IPN Orsay [9] and then shipped to Jefferson Lab (JLab), along with the components of the support structure. The support structure consists of six separate aluminum arches that are fastened together to form a ring, which is in turn attached to the solenoid by means of stainless-steel brackets. The support structure was installed first onto the CLAS12 solenoid, and then the 24 blocks of the CND were inserted, one by one, and secured onto the structure. The PMTs, within their shields, were then connected to the end of the light guides, to which they were coupled with optical grease. Figure 2 shows the detector after its installation.

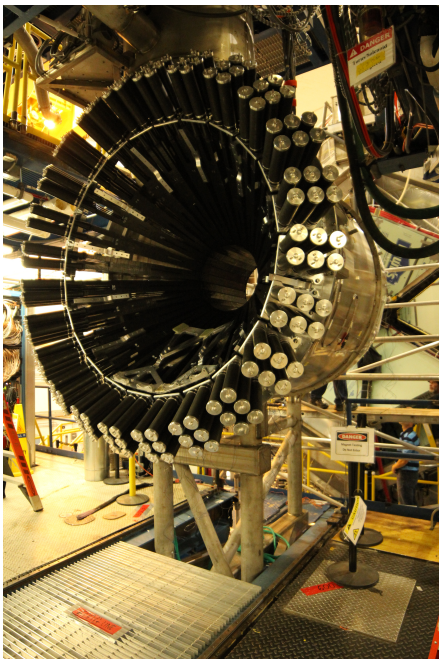

Figure 2: The CND as installed in the CLAS12 solenoid.

5. Electronics and Readout

The completely resistive high-voltage dividers of the CND were designed following the voltage distribution ratio suggested by Hamamatsu. The tube-base assembly was developed at IPN Orsay with the aim to mechanically match the mild-steel PMT shielding, for a compact and robust design. In order to operate the PMTs, high voltages (typically in the range of 1500 V) are provided by multi-channel CAEN SY527 power supplies. The HV boards adopted for the CND are CAEN A734N (16 channels, 3 kV maximum voltage, 3 mA maximum current). The signal of each PMT is sent to an active splitter. The three splitter modules used for the CND were originally developed by IPN Orsay for the G0 experiment (Hall C, JLab) [14]. Each module is an active 64-channel splitter with unity gain, so that there is no loss of amplitude. The 64 SMA inputs are placed in the back panel. In the front panel there are 8 8-channel output connectors (DMCH) for the time signals and 4 16-channel output connectors (FASTBUS) for the charge signals. The charge signal from the splitter is sent to JLab-designed 16-channel 250 MHz VXS-based flash-ADCs (FADCs). The time signal from the splitter is sent to a constant fraction discriminator (CFD) GANELEC FCC8, originally developed for the TAPS detector in Mainz. Each CFD module is an 8-channel CAMAC unit with LEMO 00 input connectors and 2x8-pin output connectors in differential ECL. The threshold can be set for each channel individually using a manual switch or remote control, and no time-walk adjustment

Constant name	Number of constants	Units
t_{LR}	72	ns
v_{eff}	144	cm/ns
u_{t}	72	ns
$t_{\mathrm{LR_{ad}}}$	72	ns
t_{off}	72	ns
A_{L}	144	cm
MIP_{D}, MIP_{I}	144 each	no units

Table 2: The constants computed in the CND calibration. See text for details.

is required for the module. The discriminated time signal then goes to the TDC (CAEN VX1290A, 32 channels/board, 25 ps/channel resolution). In total, the read out system includes 3 splitter modules, 19 CFD modules, 5 TDC boards, and 8 FADC boards.

6. Calibration

The calibration of the CND with beam data is done in two steps: the timing calibration, which allows us to obtain effective velocities and time offsets, which are, in turn, necessary to deduce timing and position information of the hits; and the energy calibration, in which attenuation lengths and energy conversion factors are extracted. Table 2 summarizes the calibration constants necessary to reconstruct CND hits.

6.1. Timing Calibration

There are five calibration constants that must be determined as part of the CND timing calibration: the two left-right time offsets (t_{LR} and $t_{\mathrm{LR_{ad}}}$), the effective velocity (v_{eff}), the propagation time in the U-turn (u_{t}), and the global time offset with respect to the event start time (t_{off}). The calibrations of these constants must be done in the following order: t_{LR}, v_{eff}, u_{t}, $t_{\mathrm{LR_{ad}}}$, and finally t_{off}. Each of these constants is determined using charged particles from beam interactions in the target.

The raw hit times t_{LR} are obtained from the measured TDC channel using a slope constant of 0.0234 ns/channel for all channels.

The paddle in which the hit occurs must be determined before the calibration procedure can be applied. The left and right times of a hit in the left paddle (we label them as t_{LL} and t_{RL} where the first index corresponds to the paddle under examination, while the second indicates the paddle in which the primary hit happened) are given by:

$$t_{\mathrm{LL}} = t_{\mathrm{off}} + t_{\mathrm{tof}} + \frac{z}{v_{\mathrm{eff_L}}} + t_{\mathrm{S}} + \mathrm{TDC_j}, \quad (4)$$

$$t_{\mathrm{RL}} = t_{\mathrm{off}} + t_{\mathrm{tof}} - \frac{z}{v_{\mathrm{eff_L}}} + \frac{L}{v_{\mathrm{eff_L}}} + \frac{L}{v_{\mathrm{eff_R}}} + u_{\mathrm{t}} + t_{\mathrm{S}} + t_{\mathrm{off_R}} - t_{\mathrm{off_L}} + \mathrm{TDC_j}, \quad (5)$$

where t_{tof} is the time of flight extracted using the CVT [12, 13] path length information, z is the position of the hit measured from the upstream end of the paddle, L is the length of the paddle, t_{S} is the start time of the event, $t_{\mathrm{off_L}}$ and $t_{\mathrm{off_R}}$ are time offsets associated with the left and right coupled paddle, and $\mathrm{TDC_j}$ is the TDC clock jitter. Similarly if the hit happened in the right paddle one can write:

$$t_{\mathrm{LR}} = t_{\mathrm{off}} + t_{\mathrm{tof}} - \frac{z}{v_{\mathrm{eff_R}}} + \frac{L}{v_{\mathrm{eff_L}}} + \frac{L}{v_{\mathrm{eff_R}}} + u_{\mathrm{t}} + t_{\mathrm{S}} + \mathrm{TDC_j}, \quad (6)$$

$$t_{\mathrm{RR}} = t_{\mathrm{off}} + t_{\mathrm{tof}} + \frac{z}{v_{\mathrm{eff_R}}} + t_{\mathrm{S}} + t_{\mathrm{off_R}} - t_{\mathrm{off_L}} + \mathrm{TDC_j}. \quad (7)$$

Defining Δ and Δ' as:

$$\Delta = \frac{L}{v_{\mathrm{eff_L}}} - \frac{L}{v_{\mathrm{eff_R}}}, \quad (8)$$

$$\Delta' = t_{\mathrm{LX}} - t_{\mathrm{RX}} + t_{\mathrm{off_R}} - t_{\mathrm{off_L}}, \quad (9)$$

where the index X can be R or L, one can compute $\Delta' - \Delta$ for both cases (hit in the left paddle or hit in the right paddle). If the hit is in the left paddle:

$$\Delta' - \Delta = \frac{2z}{v_{\mathrm{eff_L}}} - \frac{2L}{v_{\mathrm{eff_L}}} - u_{\mathrm{t}} < 0. \quad (10)$$

If the hit is in the right paddle:

$$\Delta' - \Delta = \frac{2L}{v_{\mathrm{eff_R}}} - \frac{2z}{v_{\mathrm{eff_R}}} + u_{\mathrm{t}} > 0. \quad (11)$$

If $\Delta' < \Delta$, the paddle in which the hit happened is the left one, otherwise it is the right one. This procedure to determine the hit paddle depends on constants yet to be calibrated (v_{eff} and $t_{\mathrm{off_R}} - t_{\mathrm{off_L}}$). Therefore, at least two iterations of the calibrations of v_{eff} and $t_{\mathrm{off_R}} - t_{\mathrm{off_L}}$ are required.

6.1.1. Left-Right Timing Offset

The left-right time offset refers to the time misalignment between two coupled paddles. It is determined in two steps. The first step relies on the U-turn structure of the CND to extract an estimate of this offset t_{LR}. The second step corrects t_{LR} to obtain the *adjusted* value $t_{\mathrm{LR_{ad}}}$ by taking into account the effective velocities of both coupled paddles. There is one value of t_{LR} and $t_{\mathrm{LR_{ad}}}$ for each pair of coupled paddles.

There are two different algorithms to find t_{LR} depending on whether the data were taken with or without magnetic field of the solenoid.

- If the solenoid field is off, the U-turn light guide coupling two adjacent CND paddles induces a gap in the time difference $t_R - t_L$ plots. The t_{LR} constant is defined as the time difference value at the center of the gap.
- If the solenoid is on, "double hits" occur. When the trajectory of a charged particle bent in the solenoid field crosses two adjacent coupled paddles, the two L/R signals have very similar TDC values (see Fig. 3). Such hits induce a peak instead of a gap in the time difference plots (see Fig. 4). t_{LR} is defined as the position of this peak.

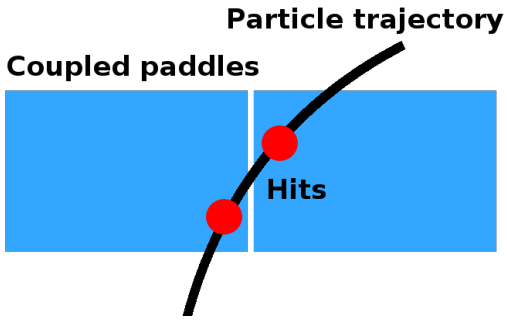

Figure 3: Double hits in the CND produced by the curved trajectory of a charged particle in the solenoid field. Both hits have similar TDC values, resulting in a peak in the time difference distribution.

The "field on" case is illustrated in Fig. 4. Typical values for the offsets are below 5 ns. t_{LR} is not used in the reconstruction, but it is nonetheless necessary to remove double hits from the subsequent calibration steps. $t_{LR_{ad}}$, defined below, is used in the reconstruction. Once t_{LR} constants have been determined, they are corrected to account for the different effective velocities of the two coupled paddles.

For hits in the left paddle, the two associated TDCs can be expressed with Eqs. 6 and 7. $t_{LR_{ad}}$ is defined as:

$$t_{LR_{ad}} = t_{off_R} - t_{off_L}. \tag{12}$$

Then one can write:

$$\frac{t_{LL} - t_{RL}}{2} = \frac{z}{v_{eff_L}} - C_L, \tag{13}$$

where C_L is the negative of the intercept of $\frac{t_L - t_R}{2}$ vs. z, C_L and is given by:

$$C_L = \frac{L}{2 \cdot v_{eff_L}} + \frac{L}{2 \cdot v_{eff_R}} + \frac{u_t}{2} + \frac{t_{LR_{ad}}}{2}. \tag{14}$$

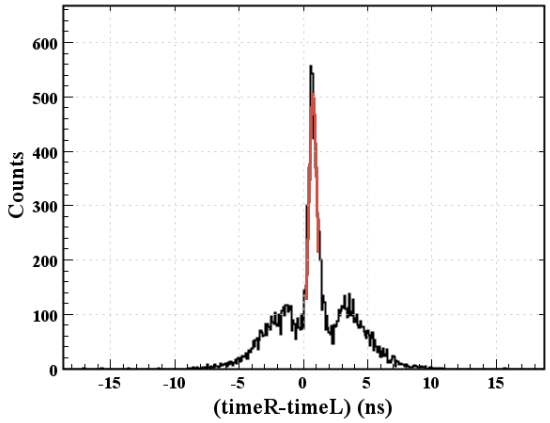

Figure 4: Left-right time difference for data with the solenoid field on: double hits, with equal TDC values, produce a peak instead of a gap.

For hits in the right paddle, the corresponding intercept C_R is given by:

$$C_R = \frac{L}{2 \cdot v_{eff_R}} + \frac{L}{2 \cdot v_{eff_L}} + \frac{u_t}{2} - \frac{t_{LR_{ad}}}{2}. \tag{15}$$

Combining Eqs. 14 and 15, $t_{LR_{ad}}$ is given by:

$$t_{LR_{ad}} = C_L - C_R. \tag{16}$$

6.1.2. *Effective Velocity*

The effective velocity v_{eff} is the speed of the light in the scintillators and the light guides. There is one v_{eff} value for each coupled paddle. v_{eff} is obtained from the following equation:

$$z = (t_L - t_R) \cdot \frac{v_{eff}}{2} + c, \tag{17}$$

where z is the z position of the hit in the CND with respect to the upstream end of the CND paddles and c is an unknown constant. z is obtained independently from the CND, using the CVT. The above equation is true for hits in the left paddles. For hits in the right paddles, the sign of the time difference must be changed. v_{eff} is extracted by fitting the $\frac{t_R - t_L}{2}$ vs. z distribution as shown in Fig. 5. For each slice in z, the position of the maximum from a Gaussian fit is plotted against z. The slope of the obtained distribution gives v_{eff}. The expected values for v_{eff} are around 16 cm/ns.

6.1.3. *U-turn Propagation Time*

The U-turn propagation time u_t is the time spent for the light to travel through the U-turn light guide. It is

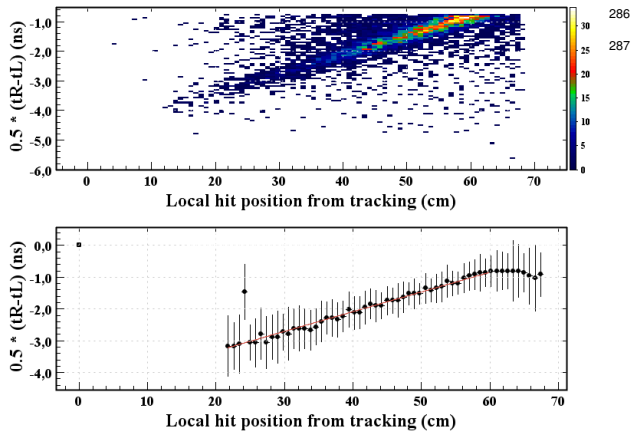

Figure 5: Plots used to determine the effective velocity for a CND paddle. The top plot shows the raw $\frac{t_R - t_L}{2}$ vs. z and the bottom plot is the distribution showing the linear fit.

used as a time offset on the indirect signal in the time and position reconstruction. There is one u_t value for each pair of paddles. The algorithm to extract u_t is very similar to the one used in the v_{eff} procedure: the intercept of the $\frac{t_R - t_L}{2}$ vs. z distribution (see Fig. 5) is extracted for both coupled paddles to determine u_t.

From the sum of the intercepts C_L in Eq. 15 and C_R in Eq. 15, u_t is obtained as :

$$u_t = C_R + C_L - L\left(\frac{1}{v_{eff_R}} + \frac{1}{v_{eff_L}}\right). \quad (18)$$

The values for u_t are typically in the range from 0.5 ns - 1.5 ns, with layer 1 values around 0.6 ns, layer 2 around 1 ns, and layer 3 around 1.4 ns.

6.1.4. Global Time Offset

The global time offset t_{off} refers to the time difference between the start time value and the vertex time computed from the CND hit time and the CVT path length information. There is one t_{off} value for each pair of coupled paddles. t_{off} is given by:

$$t_{off} = \frac{t_L + t_R}{2} - t_S - t_{tof} - \frac{L}{2}\cdot\left(\frac{1}{v_{eff_R}} + \frac{1}{v_{eff_L}}\right) - \frac{u_t}{2} - \frac{t_{LR_{ad}}}{2} - TDC_j, \quad (19)$$

where t_{tof} is calculated using CVT information assuming the particles are pions. For this, a negative charge is required, as most of the negative particles in the Central Detector are pions. The position of the peak of the above distribution gives t_{off} (see Fig. 6). These values depend mainly on the start time t_S, which is calculated using the CLAS12 Forward Time-of-Flight System (FTOF) [15]. The variations of t_{off} between different pairs of paddles are typically below 10 ns.

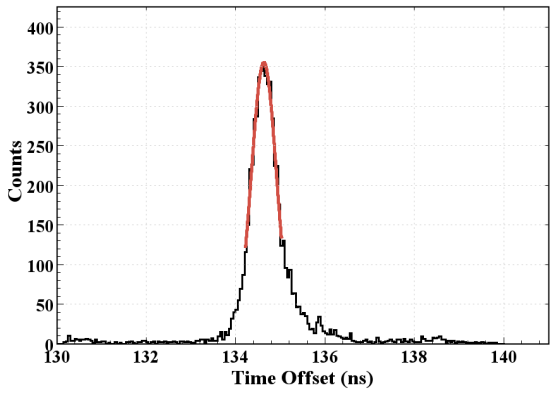

Figure 6: Plot used to determine the global time offset. The distribution is fit with a Gaussian and the position the peak corresponds to t_{off}.

6.2. Energy Calibration

There are three calibration constants for the energy determination in each paddle of the CND: the attenuation length (A_L), the ADC-to-energy constants for direct minimum-ionizing particles (MIPs) (MIP_D), and the ADC-to-energy constants for indirect MIPs (MIP_I). These three calibration steps can be performed almost independently from the timing calibration, however, $t_{LR_{ad}}$ is needed to determine if an ADC signal is direct or indirect (i.e. the hit happened in the considered paddle or in its coupled partner).

6.2.1. Attenuation Length

The attenuation length A_L accounts for the light attenuation along the length of the scintillators and light guides. There is an A_L value for each paddle. For hits in the left paddle, the two associated ADCs can be written as:

$$ADC_L = \frac{E}{E_0}\cdot MIP_D \cdot e^{\frac{-z}{A_L}}, \quad (20)$$

$$ADC_R = \frac{E}{E_0}\cdot MIP_I \cdot e^{\frac{-(L-z)}{A_L}}, \quad (21)$$

where MIP_D and MIP_I are constants defined in the Section 6.2.2 (MIP_I includes the effect of the light attenuation in the R paddle), E is half the energy deposited by the particle in the scintillator, and E_0 is half the energy deposited by a MIP in the scintillators. E_0 is given by:

$$E_0 = \frac{h \cdot 2.001}{2}\text{MeV}, \quad (22)$$

where h is the thickness of each scintillator. All the above equations are valid for hits in the left paddles, while for hits in the right paddles, the corresponding equations are obtained by switching the L/R indices. From Eqs. 20 and 21 the following relation is derived:

$$ln(ADC_{\rm L}/ADC_{\rm R}) = c - \frac{2 \cdot z}{A_{\rm L}}, \qquad (23)$$

where c is a constant depending on $MIP_{\rm D}$, $MIP_{\rm I}$, and L. $A_{\rm L}$ is given by the slope of the distribution in Eq. 23 as shown in Fig. 7. Values for $A_{\rm L}$ are typically around 150 cm.

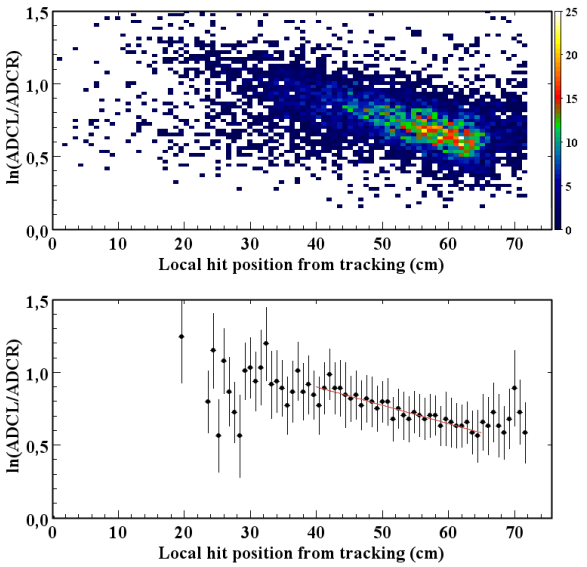

Figure 7: Plots used to determine $A_{\rm L}$. The top plot shows the raw $ln(ADC_{\rm L}/ADC_{\rm R})$ vs. z distribution for one pair of paddles. Slices in z are fit with a Gaussian and the mean is the plotted against z. The corresponding distribution and its associated linear fit is shown in the bottom plot.

6.2.2. Energy Calibration Parameters

The final step of the calibration of the CND is the determination of the energy conversion parameters $MIP_{\rm D}$ and $MIP_{\rm I}$. There are two energy parameters for each paddle, thus there are four energy parameters for each pair of coupled paddles, denoted as $MIP_{\rm DL}$, $MIP_{\rm IL}$, $MIP_{\rm DR}$, $MIP_{\rm IR}$.

In the following, we only consider a hit in the left paddle. Equations for hits in right paddles are obtained by switching the L/R indices. For hits in the left paddle, only $MIP_{\rm DL}$ and $MIP_{\rm IL}$ can be obtained. In the following they are referred to as $MIP_{\rm D}$ and $MIP_{\rm I}$. From Eqs. 20 and 21, one gets:

$$ln\left(\frac{ADC_{\rm L}}{ADC_{\rm R}}\right) = ln\left(\frac{MIP_{\rm D}}{MIP_{\rm I}}\right) + \frac{L}{A_{\rm L}} - \frac{2 \cdot z}{A_{\rm L}} \qquad (24)$$

$$\sqrt{ADC_{\rm L} \cdot ADC_{\rm R}} = \frac{E}{E_0} \cdot \sqrt{MIP_{\rm D} \cdot MIP_{\rm I}} e^{-\frac{L}{2 \cdot A_{\rm L}}}. \qquad (25)$$

From Eq. 24, the intercept of the $ln\left(\frac{ADC_{\rm L}}{ADC_{\rm R}}\right)$ vs. z distribution (Fig. 7) gives the ratio $\frac{MIP_{\rm D}}{MIP_{\rm I}}$. The product $MIP_{\rm D} \cdot MIP_{\rm I}$ is obtained using Eq. 25 after filtering MIPs and correcting for the path traveled by the MIP in the scintillators. Indeed for MIPs, E can be written as:

$$E = \frac{path}{h} \cdot E_0, \qquad (26)$$

where *path* is the path length traveled by the MIP in the scintillator, which is obtained using the CVT tracking information by extrapolating the particle trajectory at the radius of the CND hit. Selecting MIPs and correcting for the path length removes the energy dependence from Eq. 25, which becomes:

$$\sqrt{ADC_{\rm L} \cdot ADC_{\rm R}} = \frac{path}{h} \cdot \sqrt{MIP_{\rm D} \cdot MIP_{\rm I}} e^{-\frac{L}{2 \cdot A_{\rm L}}}. \qquad (27)$$

The distribution of $\sqrt{ADC_{\rm L} \cdot ADC_{\rm R}} \cdot \frac{h}{path}$ is fit with a Landau function and the position of the peak p is extracted as shown in Fig. 8. $MIP_{\rm D}$ and $MIP_{\rm I}$ are given by:

$$MIP_{\rm D} = \sqrt{e^{i - \frac{L}{A_{\rm L}}} \cdot e^{\frac{L}{A_{\rm L}}} \cdot p^2}, \qquad (28)$$

$$MIP_{\rm I} = \sqrt{e^{-\left(i - \frac{L}{A_{\rm L}}\right)} \cdot e^{\frac{L}{A_{\rm L}}} \cdot p^2}, \qquad (29)$$

where i and p are the intercept and peak position defined above. $MIP_{\rm D}$ and $MIP_{\rm I}$ are typically around 2000 and 500, respectively.

7. Simulation

In order to study the performance of the CND, its geometry and response were included in the CLAS12 Geant4-based simulation package, GEMC [16]. The Birks effect, for which the number of optical photons produced for a given energy deposition in the scintillator depends on the particle type, and the hit digitization for the CND, were introduced in GEMC. The timing resolution and the energy loss due to the U-turn geometry were included in the simulation using the values measured in the cosmic-ray tests. Details on the digitization

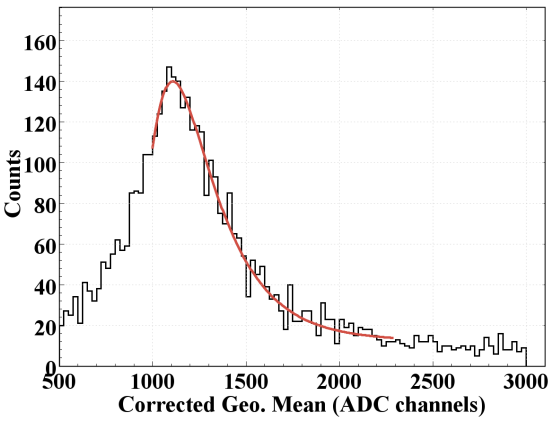

Figure 8: $\sqrt{ADC_{\rm L} \cdot ADC_{\rm R}} \cdot \frac{h}{path}$ distribution fit with a Landau function. The events in this plot are identified as MIPs by requiring a pion. The particle identification is performed requiring a negative charge, as most negatively charged particles in the Central Detector are pions.

and on the hit and event reconstruction are explained in Ref. [16] and Ref. [17], respectively.

Simulations of the n-DVCS reaction were run to evaluate the efficiency of the CND for neutrons and its angular and momentum resolutions. Figure 9 shows the neutron detection efficiency as a function of neutron momentum. It is fairly constant and has an average value of roughly 9%. The angular resolution σ_θ, obtained via Gaussian fits of the difference between the generated and reconstructed θ, is also fairly constant as a function of neutron momentum, with an average value of about 2.5°. The resolution on the azimuthal angle is directly connected to the total number of scintillator bars along ϕ with the angular size of each bar $\Delta\phi$=7.5°, σ_ϕ is given by $\Delta\phi/2 = 3.75°$. The resolution on the neutron momentum, which is obtained knowing β and having performed the particle identification, according to the formula

$$p = \frac{\beta \cdot m_n}{\sqrt{1-\beta^2}}, \tag{30}$$

is also strictly connected to the time resolution. The average relative momentum resolution σ_p/p is ~8%. No appreciable variation of momentum resolution was observed as a function of the neutron polar angle.

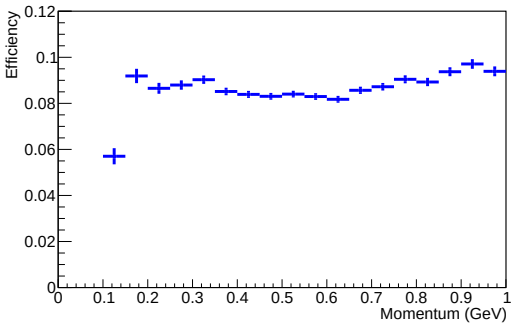

Figure 9: Simulation results for the efficiency for the detection of neutrons in the CND from the n-DVCS reaction.

Since the charged particles passing through the CND will be vetoed by the CVT, the only particles that could be mistaken for neutrons in the CND are photons. The efficiency of the CND for photons has been estimated by simulations, and it is slightly larger than for neutrons (on the order of 15%, having little energy dependence). Neutrons can be discriminated from photons by means of their β. Therefore, the β distributions that can be obtained with the CND for neutrons and photons were studied with the help of the GEMC simulation. Neutrons and photons of momenta varying between 0.1 and 1 GeV were generated at a fixed azimuthal angle ($\phi = 3.75°$). Figure 10 shows the comparison between the β distributions obtained for neutrons of various momenta (0.2, 0.4, 0.7, and 1 GeV) and for 1-GeV photons. All particles in this plot were emitted at $\theta = 60°$. A small portion of the neutrons having momentum of 1 GeV can be taken as photons, as their β distributions begin to overlap, while the n/γ separation is clear for lower momenta — which corresponds to most of the range of interest for n-DVCS, as only about 8% of the events are expected to have $p_n > 0.9$ GeV.

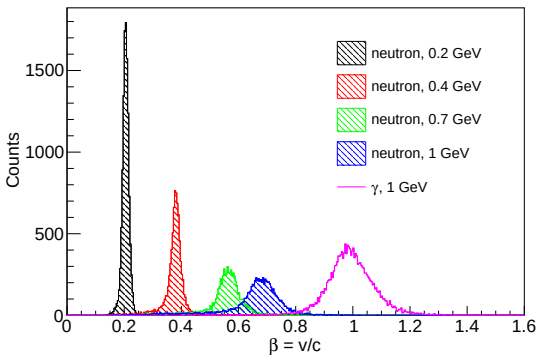

Figure 10: Simulation results for the β distributions for neutrons with $p_n = 0.2$ GeV (black), $p_n = 0.4$ GeV (red), $p_n = 0.7$ GeV (green), $p_n = 1$ GeV (blue), and photons with $E = 1$ GeV (purple). The threshold on the deposited energy is 3 MeV. The plot shows all reconstructed particles integrated over ϕ. Equal neutron and photon yields were assumed.

8. Performance

After the calibration constants are determined, the timing, position, and deposited energy of each hit are reconstructed, and clusters are formed grouping hits according to their position and timing [17].

Data taken during the first CLAS12 experiments on hydrogen and deuterium targets, and with various beam energies (7.5 and 10.6 GeV), were analyzed to verify the performance of the CND.

The timing performance for the three layers of the CND is illustrated in Fig. 11, showing the vertex time difference v_t for selected negative tracks, assumed to be all pions, integrated over all sectors defined as

$$v_t = t_{\mathrm{CND}} - (t_{\mathrm{S}} - vz_{corr}) - \frac{P_L}{c \cdot \beta}, \tag{31}$$

where t_{CND} is the mean time reconstructed from the L and R paddles, t_{S} is the event start time determined by the RF bucket matched with the FTOF vertex time, vz_{corr} accounts for the actual z position of the interaction vertex, P_L is the path length from the event vertex to the CND, and

$$\beta = \frac{p}{\sqrt{p^2 + m^2}}, \tag{32}$$

with p the momentum measured by the CVT, and m the pion mass. The distribution of v_t is centered at 0. From the width of the v_t distribution the timing resolution of each CND paddle convoluted with the CVT resolution can be determined as:

$$\sigma_t = \sqrt{\sigma_{v_t}^2 - \sigma_{t_S}^2} = 185 \text{ ps}, \tag{33}$$

assuming the resolution of the start time σ_{t_S}=20 ps [15]. The timing resolution for the 144 individual CND counters is shown in Fig. 12. Its average (indicated by the horizontal line) is around 185 ps, which is more than the average148 ps intrinsic timing resolution measured with cosmic rays [9]. This discrepancy is due to multiple factors, such as the current, not fully optimized, quality of the calibrations and reconstruction, as well as the uncertainty of the path length and on the other non-CND contributions to Eq. 31.

The position reconstruction performance of the CND is shown in Fig. 13, which displays the difference between the z coordinate (along the beamline) computed by the CND and by the CVT for negative tracks in all three layers of the CND integrated over all paddles. Its Gaussian width is ∼3 cm, corresponding roughly to 4° in polar-angle resolution. This corresponds to the convolution of the angular resolutions of the CND and CVT.

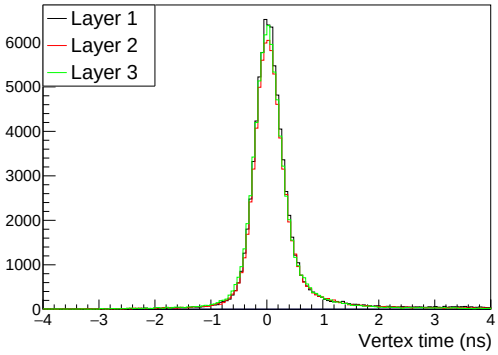

Figure 11: Difference between the vertex time computed combining CND and CVT information with the start time computed by the FTOF for negative tracks in all the three layers of the CND integrated over all paddles.

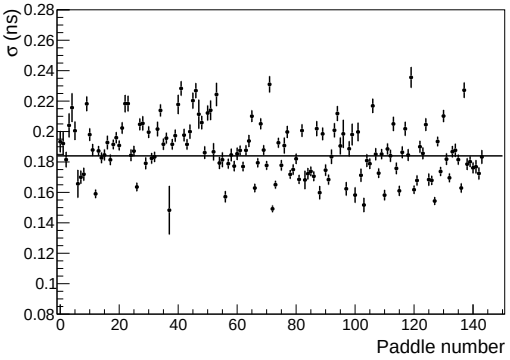

Figure 12: Timing resolution for each CND counter convoluted with the CVT resolution.

Figure 14 shows the energy deposited divided by path length for selected MIPs. It peaks at around the expected value of 2.001 MeV/cm.

8.1. Neutron Detection Efficiency

The exclusive reaction $ep \rightarrow e'n\pi^+$ was analyzed to evaluate the neutron detection efficiency of the CND. The data used were taken with a 7.5-GeV electron beam incident on a liquid-hydrogen target. Events with an electron and a π^+ in the CLAS12 Forward Detector were selected. The missing mass of the $e'\pi^+X$ system is plotted versus β_X in Fig. 15. The missing particle is required to be in the CLAS12 Central Detector ($\theta > 40°$). The effect of this selection is shown in Fig. 15. We apply an additional cut on β of the missing neutron

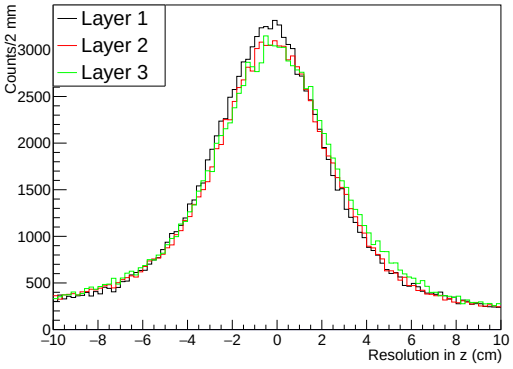

Figure 13: Difference between the z coordinate (along the beamline) computed by the CND and the CVT,for negative tracks in all three CND layers integrated over all paddles.

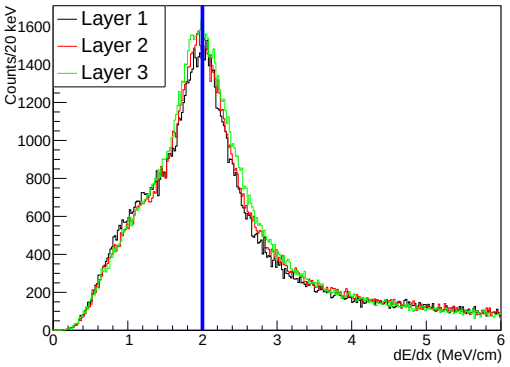

Figure 14: dE/dx for MIPs in the three layers of the CND integrated over all sectors. The blue line indicates the nominal value for the expected energy deposit of a MIP in a centimeter of plastic scintillator.

$(0.2 < \beta_X < 0.8)$. From this set of $ep \rightarrow e'(n)\pi^+$ events, events with a neutron identified by the CND (CND cluster with $E_{dep} > 2.5$ MeV, no associated CVT tracks, $\beta < 0.8$) were selected. If multiple neutron candidates were detected by the CND, the neutron with the smallest momentum separation from the missing neutron was kept. A cut on $\beta > 0.2$ was applied to remove out-of-time hits that could be mistaken as neutrons. Finally, the detected neutron and the missing neutron azimuthal angle difference is constrained to be less than 20°.

The efficiency was measured in bins of missing neutron polar angle and as a function of missing momentum. For each bin in polar angle and momentum, the efficiency is defined as the ratio of events with a detected neutron to the number of missing neutron events. The result is shown in Fig. 16. The detection efficiency extracted from this method is consistent with simulation predictions and with the design specifications of the CND.

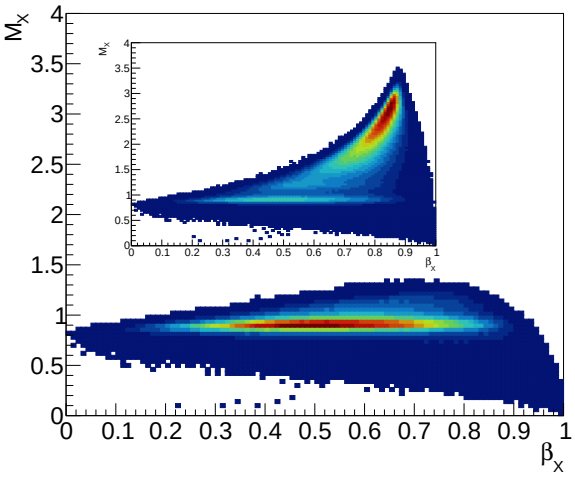

Figure 15: Missing mass M_X versus β_X of the $ep \rightarrow e'\pi^+X$ reaction. The outer plot shows the effect of selecting events where the missing particle X is emitted in the CLAS12 Central Detector.

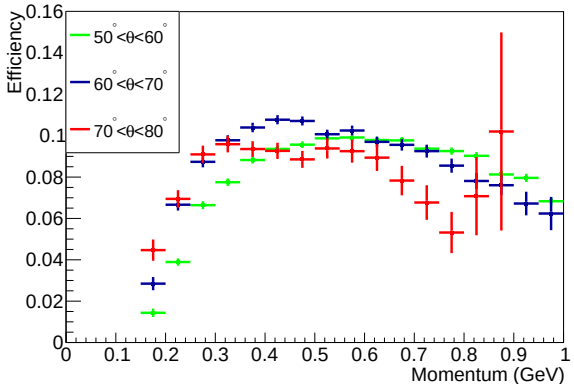

Figure 16: Neutron detection efficiency of the CND as a function of momentum for three bins in polar angle.

9. Conclusions

This article presents the requirements, the design, the calibration and reconstruction procedures, and the performance of the Central Neutron Detector for CLAS12. It consists of a barrel of three layers of scintillators

coupled at their downstream ends with U-turn light guides and read out at their upstream ends by conventional PMTs connected to the bars via 1-m-long bent light guides and placed in the fringe field region of the CLAS12 solenoid. The performance measured with beam data, which agree with the results of our Geant4-based simulations, show that the efficiencies obtainable with this detector and its photon-rejection capabilities allow for the collection of good statistics on the beam-spin asymmetry for the n-DVCS reaction over a wide phase space, using the allocated beam time for CLAS12 with a deuterium target [2]. This detector will also be used in other n-DVCS experiments [3], and whenever the detection of the recoil neutron may be required (e.g. the excited nucleon N^* program or all of the deeply virtual meson production reactions on the neutron).

10. Acknowledgments

This work was supported by IN2P3-CNRS (France) and European (Sixth Framework Program I3-HP) funds. This material is also based upon work supported by the U.S. Department of Energy, Office of Science, Office of Nuclear Physics under contract DE-AC05-06OR23177.

[1] V. D. Burkert, et al., The CLAS12 Spectrometer at Jefferson Laboratory, to be published in Nucl. Inst. and Meth. A, (2020) (see this issue).

[2] S. Niccolai, et al., Deeply virtual Compton scattering on the neutron with CLAS12 at 11 GeV, Jefferson Lab experiment E12-11-003.

[3] S. Niccolai, et al., Deeply virtual Compton scattering on the neutron with a longitudinally polarized deuteron target, Jefferson Lab experiment E12-06-109a.

[4] D. Muller, D. Robaschik, B. Geyer, F. M. Dittes, J. Horejosi, Wave functions, evolution equations and evolution kernels from light ray operators of QCD, Fortsch. Phys. 42 (1994) 101–141. arXiv:hep-ph/9812448, doi:10.1002/prop.2190420202.

[5] X.-D. Ji, Gauge-Invariant Decomposition of Nucleon Spin, Phys. Rev. Lett. 78 (1997) 610–613. arXiv:hep-ph/9603249, doi:10.1103/PhysRevLett.78.610.

[6] A. V. Radyushkin, Scaling limit of deeply virtual Compton scattering, Phys. Lett. B380 (1996) 417–425. arXiv:hep-ph/9604317, doi:10.1016/0370-2693(96)00528-X.

[7] G. Asryan, et al., The CLAS12 Forward Electromagnetic Calorimeter, to be published in Nucl. Inst. and Meth. A, (2020) (see this issue).

[8] A. Acker, et al., The CLAS12 Forward Tagger, to be published in Nucl. Inst. and Meth. A, (2020) (see this issue).

[9] S. Niccolai, et al., The central neutron detector for CLAS12, Nucl. Instrum. Meth. A904 (2018) 81–92. doi:10.1016/j.nima.2018.07.029.

[10] D. S. Carman, et al., The CLAS12 Central Time-of-Flight System, to be published in Nucl. Inst. and Meth. A, (2020) (see this issue).

[11] R. Fair, et al., The CLAS12 Superconducting Magnets, to be published in Nucl. Inst. and Meth. A, (2020) (see this issue).

[12] M. A. Antonioli, et al., The CLAS12 Silicon Vertex Tracker, to be published in Nucl. Inst. and Meth. A, (2020) (see this issue).

[13] A. Acker, et al., The CLAS12 MicroMegas Tracker, to be published in Nucl. Inst. and Meth. A, (2020) (see this issue).

[14] D. Androic, et al., The G0 Experiment: Apparatus for Parity-Violating Electron Scattering Measurements at Forward and Backward Angles, Nucl. Instrum. Meth. A646 (2011) 59–86. arXiv:1103.0761, doi:10.1016/j.nima.2011.04.031.

[15] D. S. Carman, et al., The CLAS12 Forward Time-of-Flight System, to be published in Nucl. Inst. and Meth. A, (2020) (see this issue).

[16] M. Ungaro, et al., The CLAS12 Geant4 Simulation, to be published in Nucl. Inst. and Meth. A, (2020) (see this issue).

[17] V. Ziegler, et al., The CLAS12 Software Framework and Event Reconstruction, to be published in Nucl. Inst. and Meth. A, (2020) (see this issue).

LaTeX Source Files

Click here to download LaTeX Source Files: cnd.tar

Figure1

Click here to download high resolution image

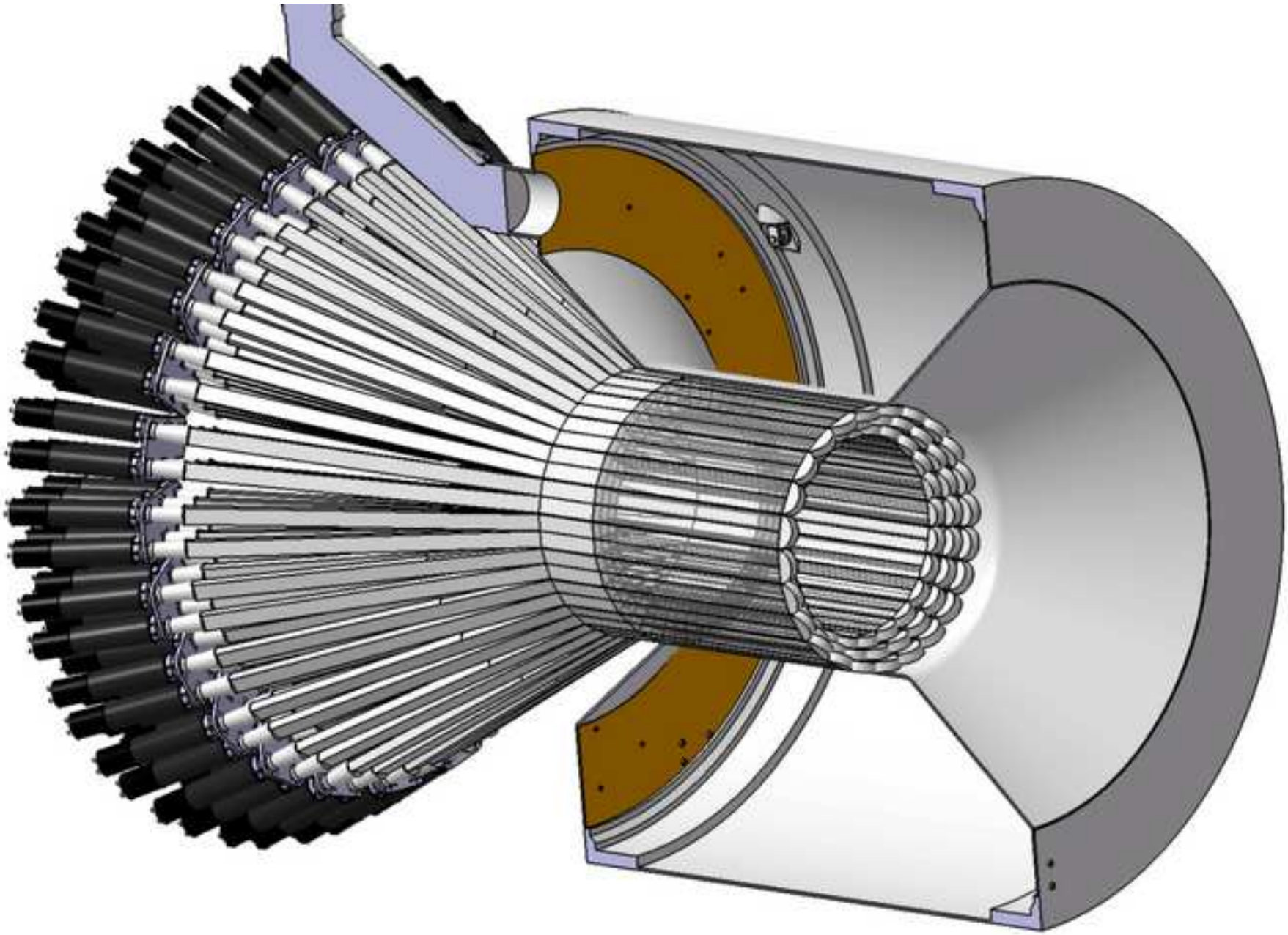

Figure2

Click here to download high resolution image

Figure3
Click here to download high resolution image

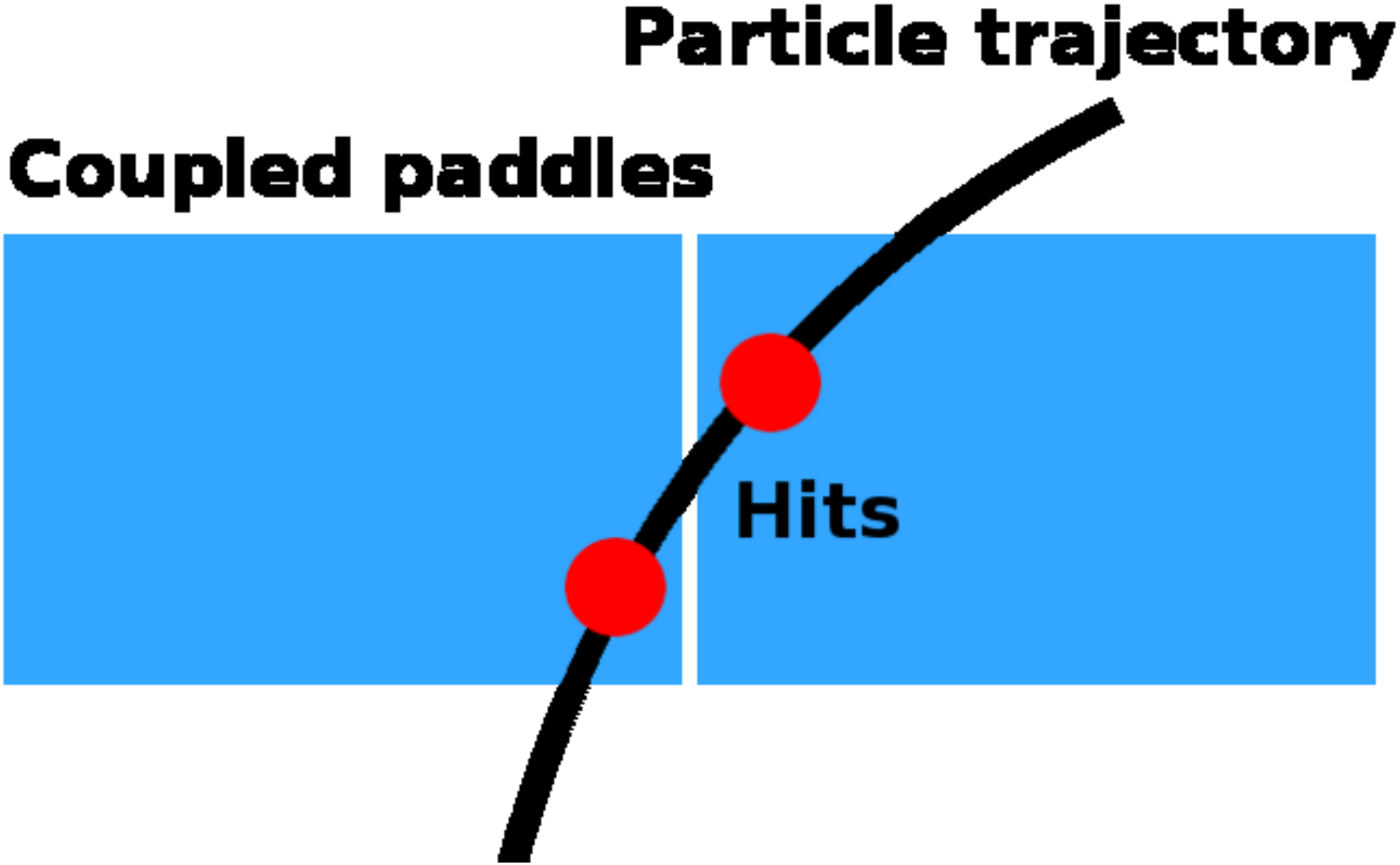

Figure4

Click here to download high resolution image

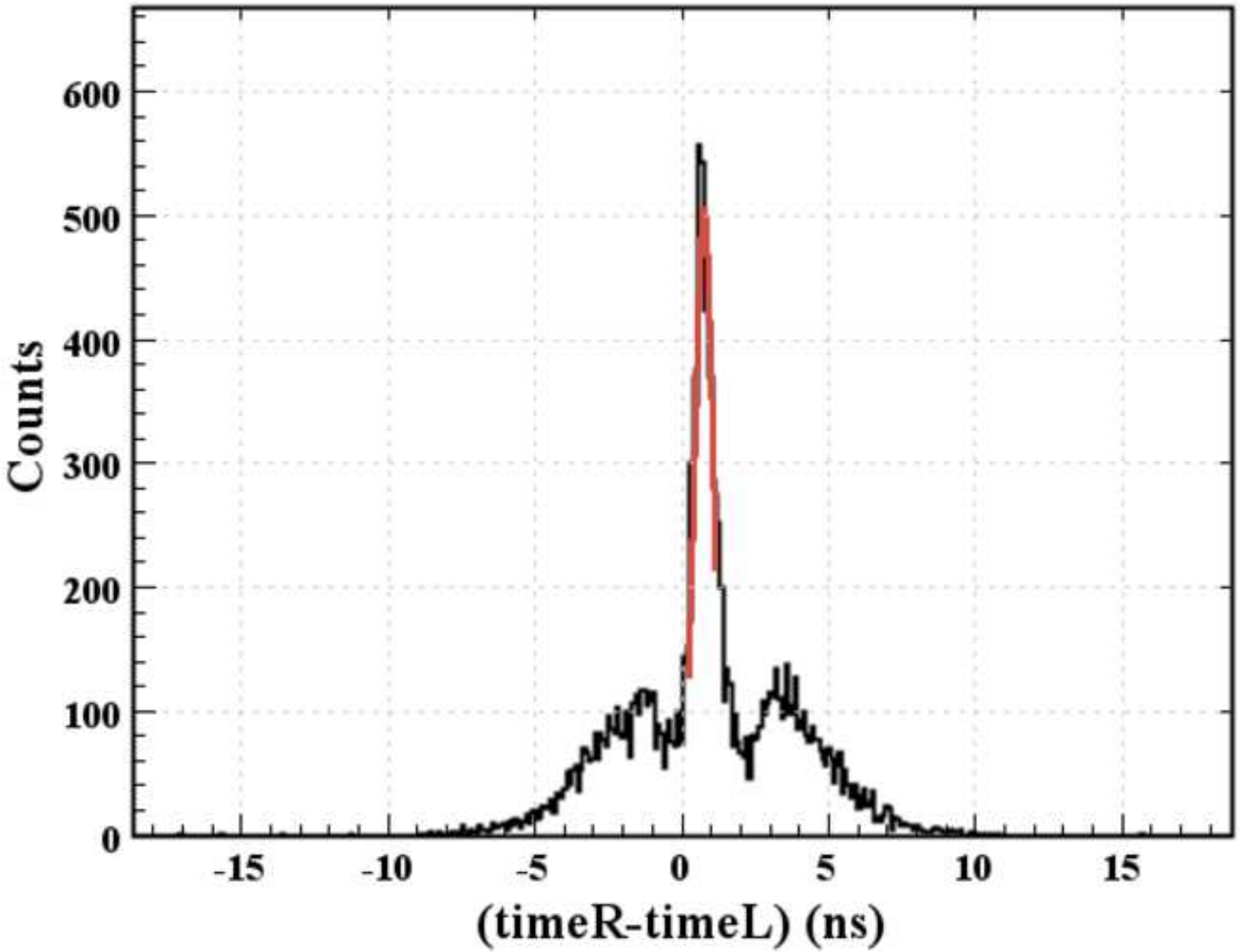

Figure5

Click here to download high resolution image

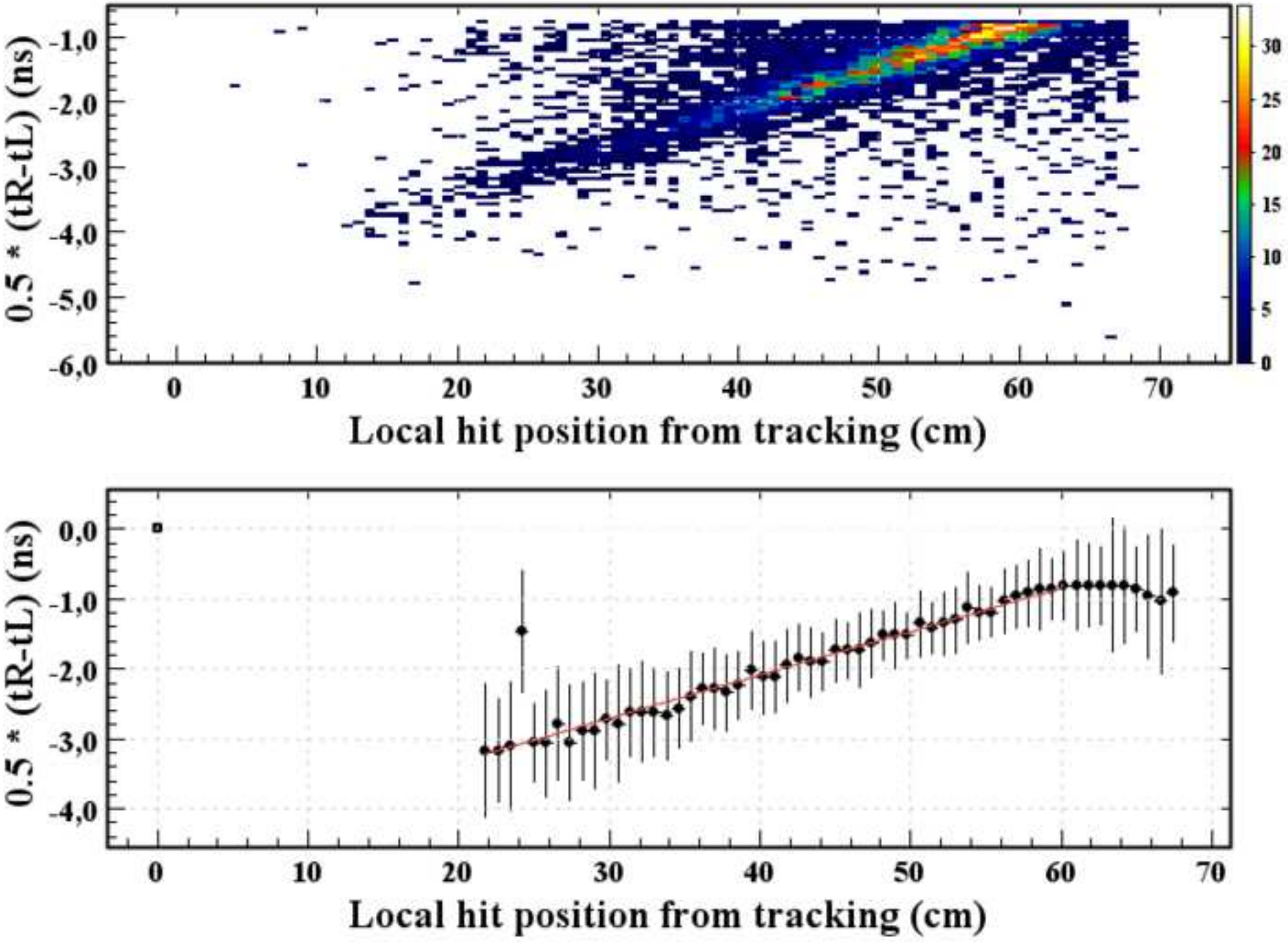

Figure6

Click here to download high resolution image

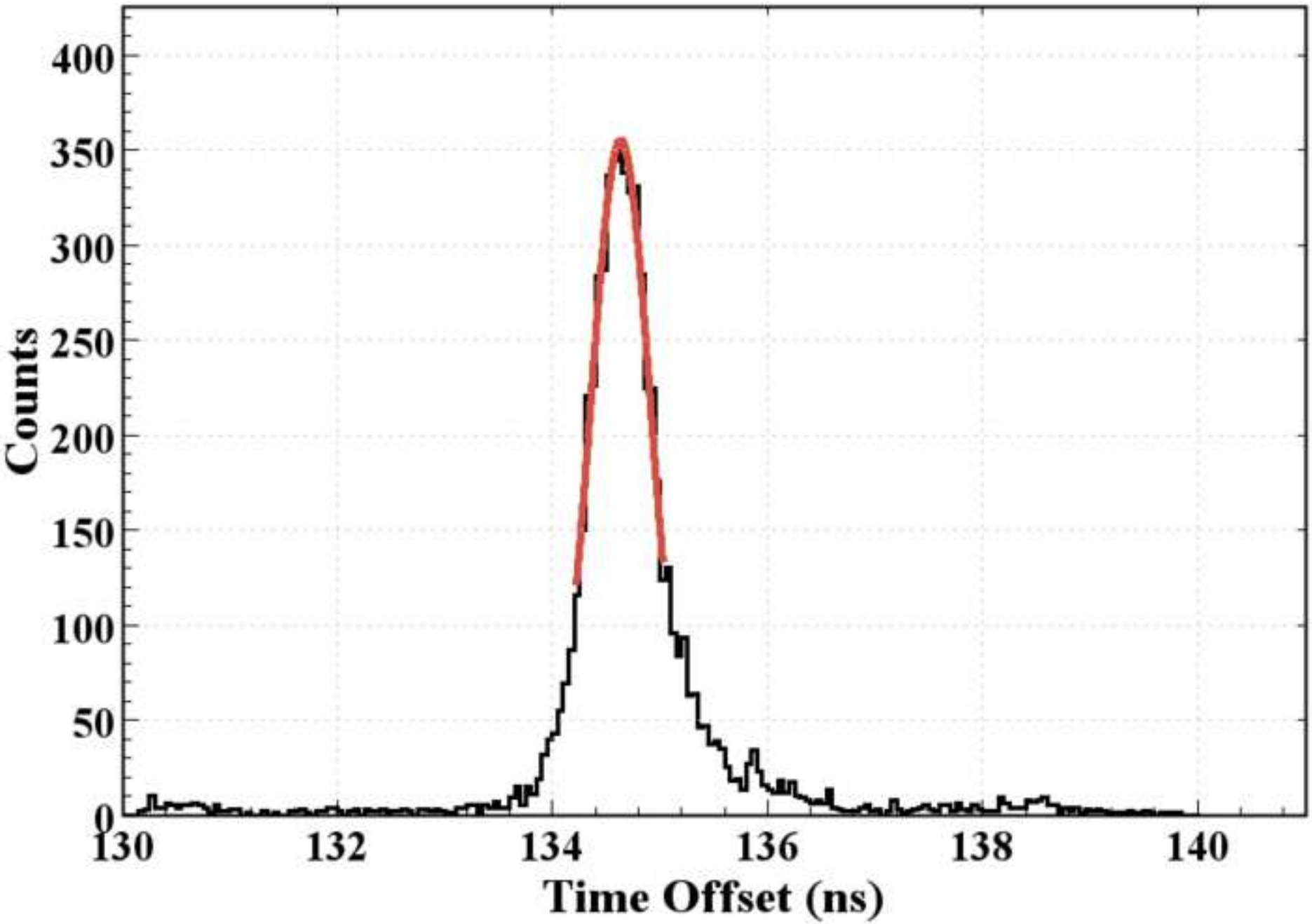

Figure7

Click here to download high resolution image

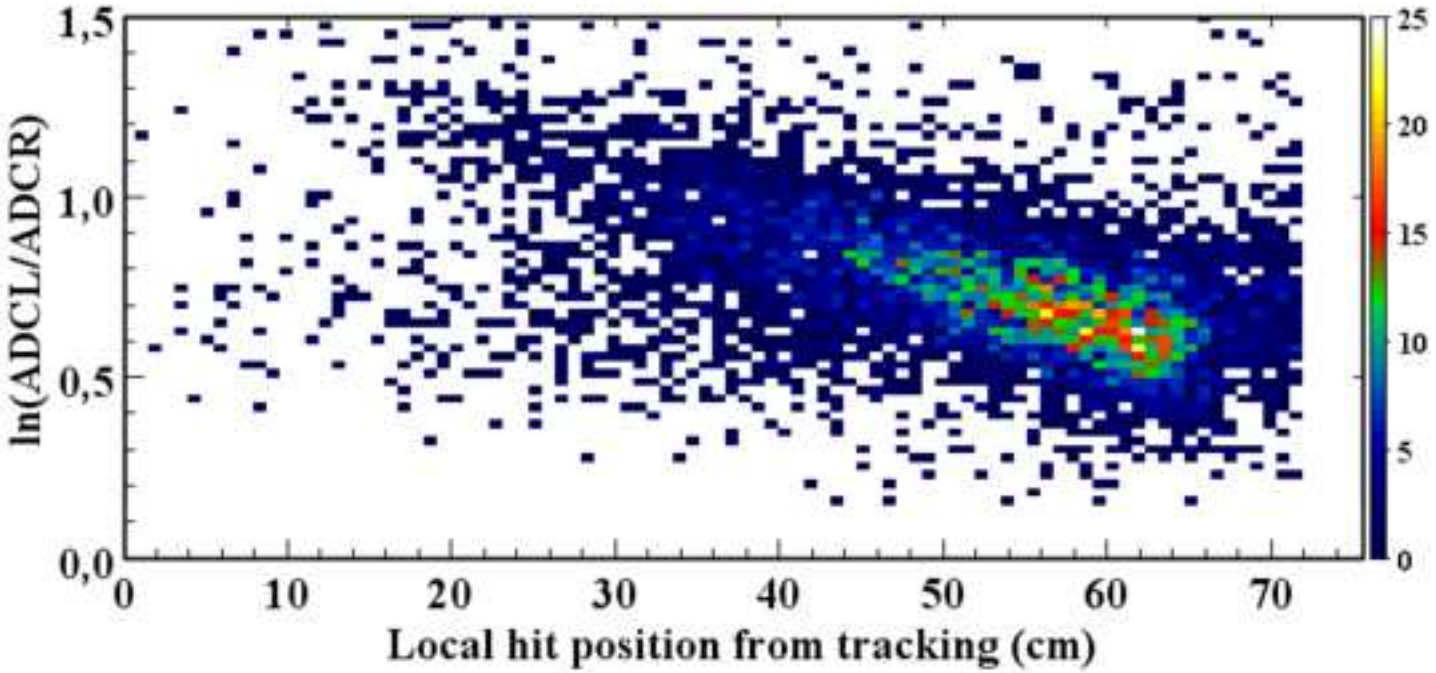

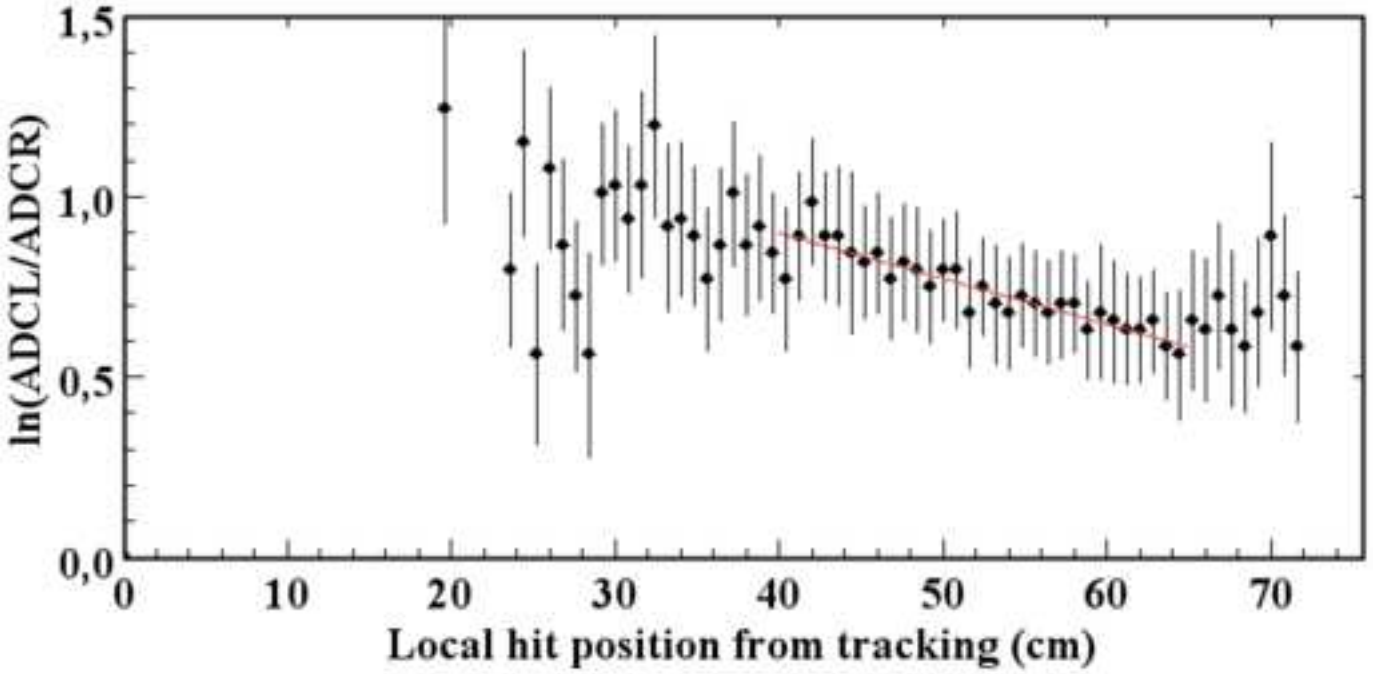

Figure8

Click here to download high resolution image

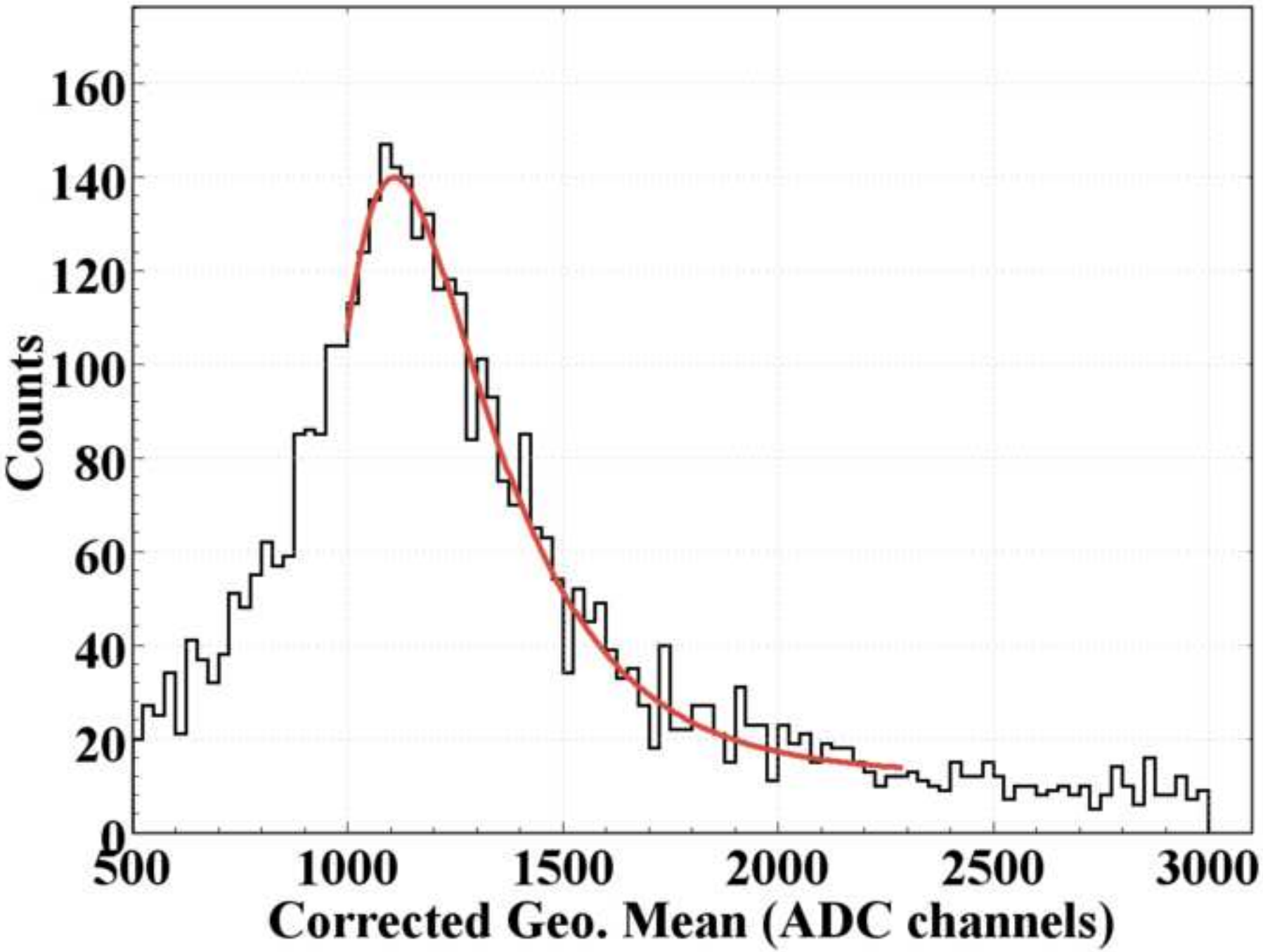

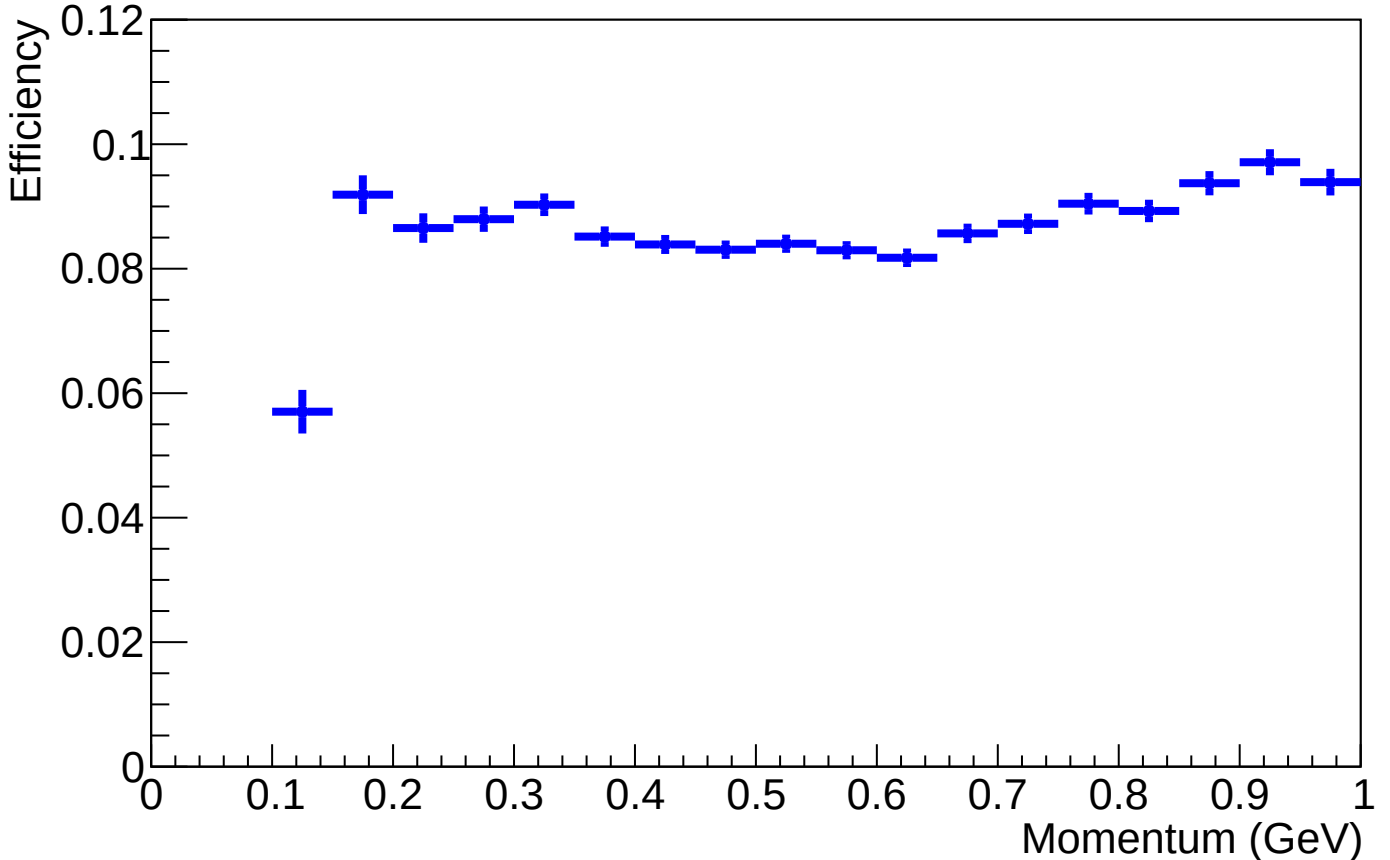
Efficiency
0.12
0.1
0.08
0.06
0.04
0.02
0
0
0.1
0.2
0.3
0.4
0.5
0.6
0.7
0.8
0.9
1
Momentum (GeV)

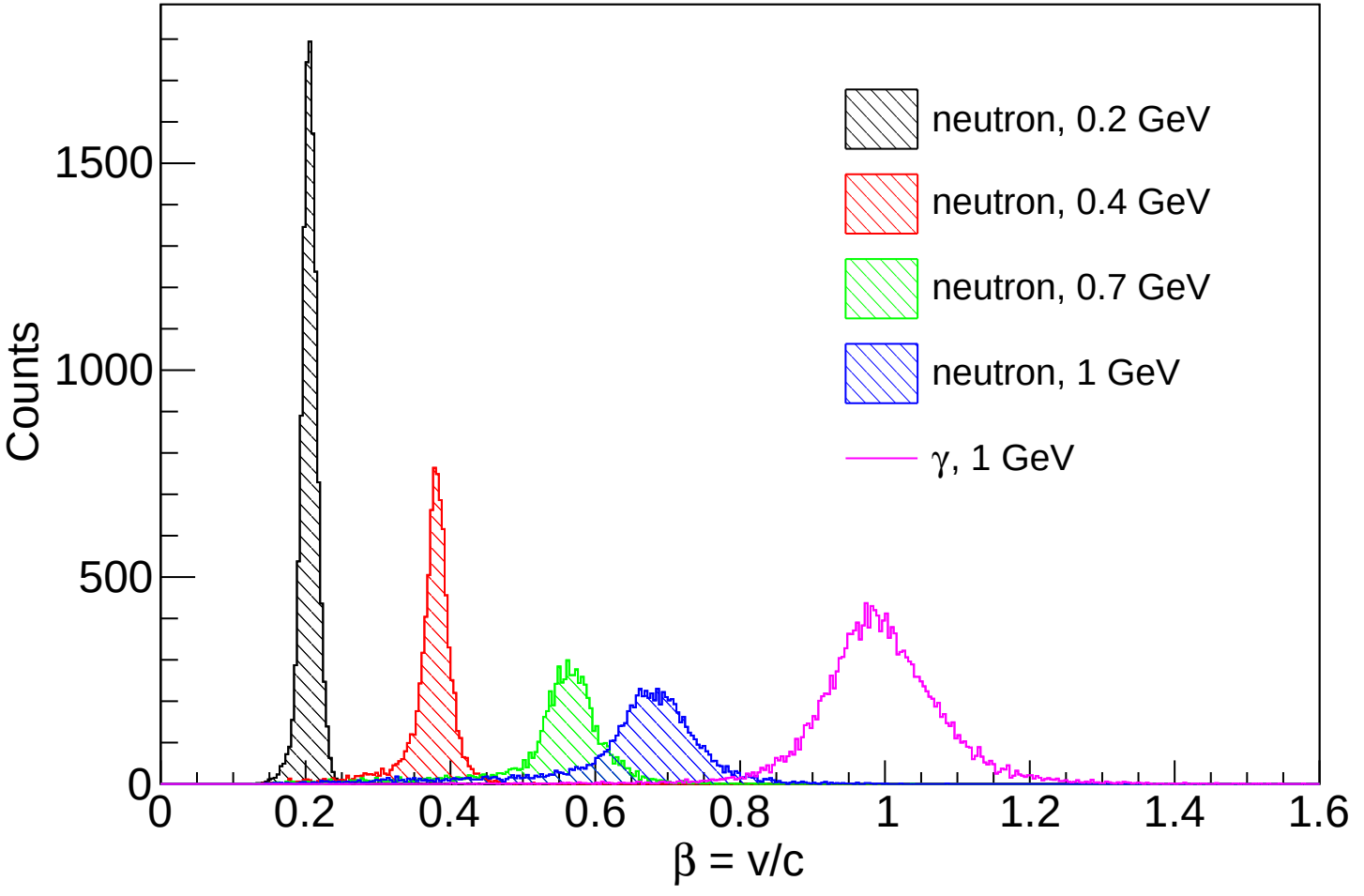
neutron, 0.2 GeV
neutron, 0.4 GeV
neutron, 0.7 GeV
neutron, 1 GeV
γ, 1 GeV
Counts
0
500
1000
1500
0
0.2
0.4
0.6
0.8
1
1.2
1.4
1.6
β = v/c

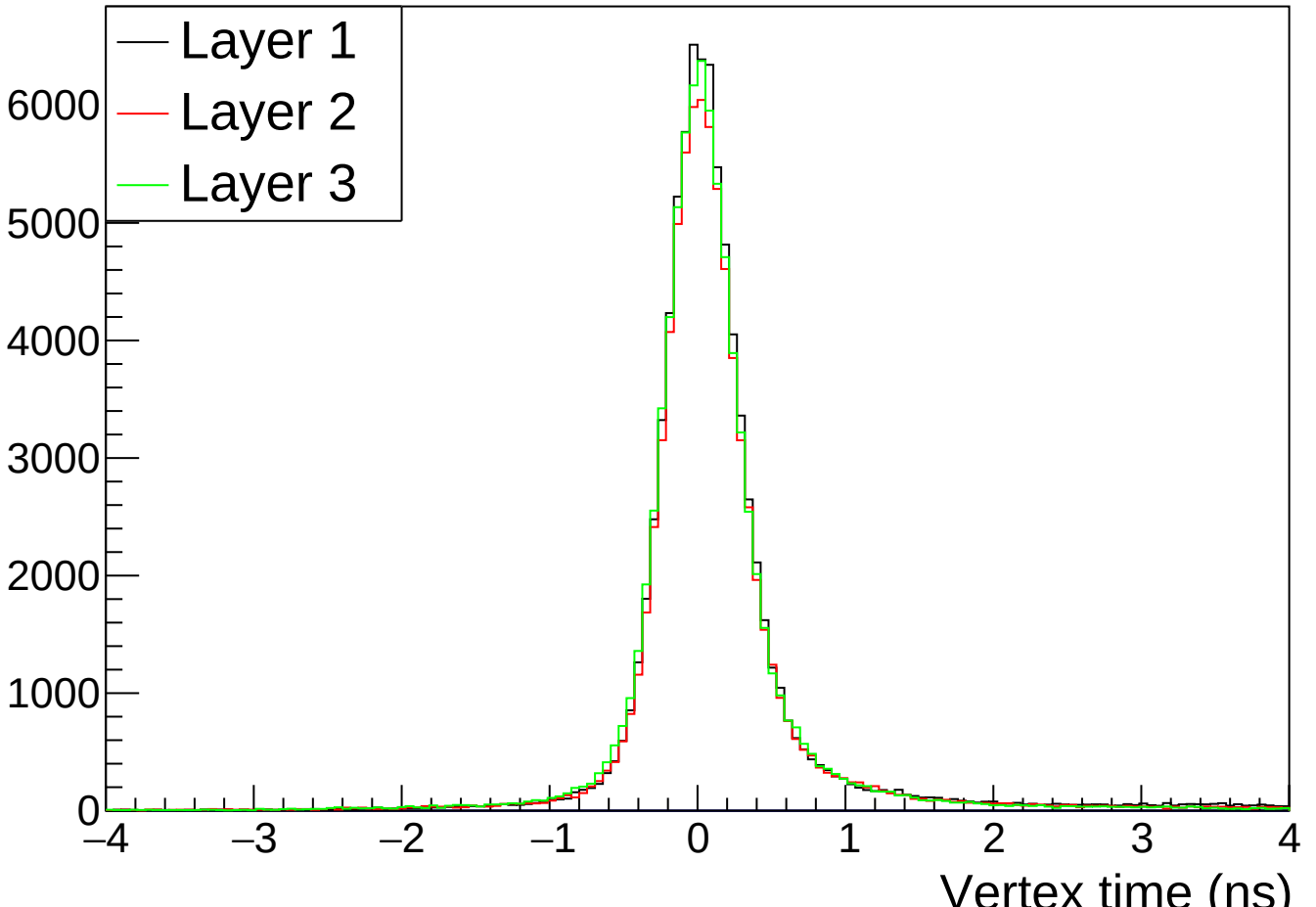
Layer 1
Layer 2
Layer 3
6000
5000
4000
3000
2000
1000
0
–4
–3
–2
–1
0
1
2
3
4
Vertex time (ns)

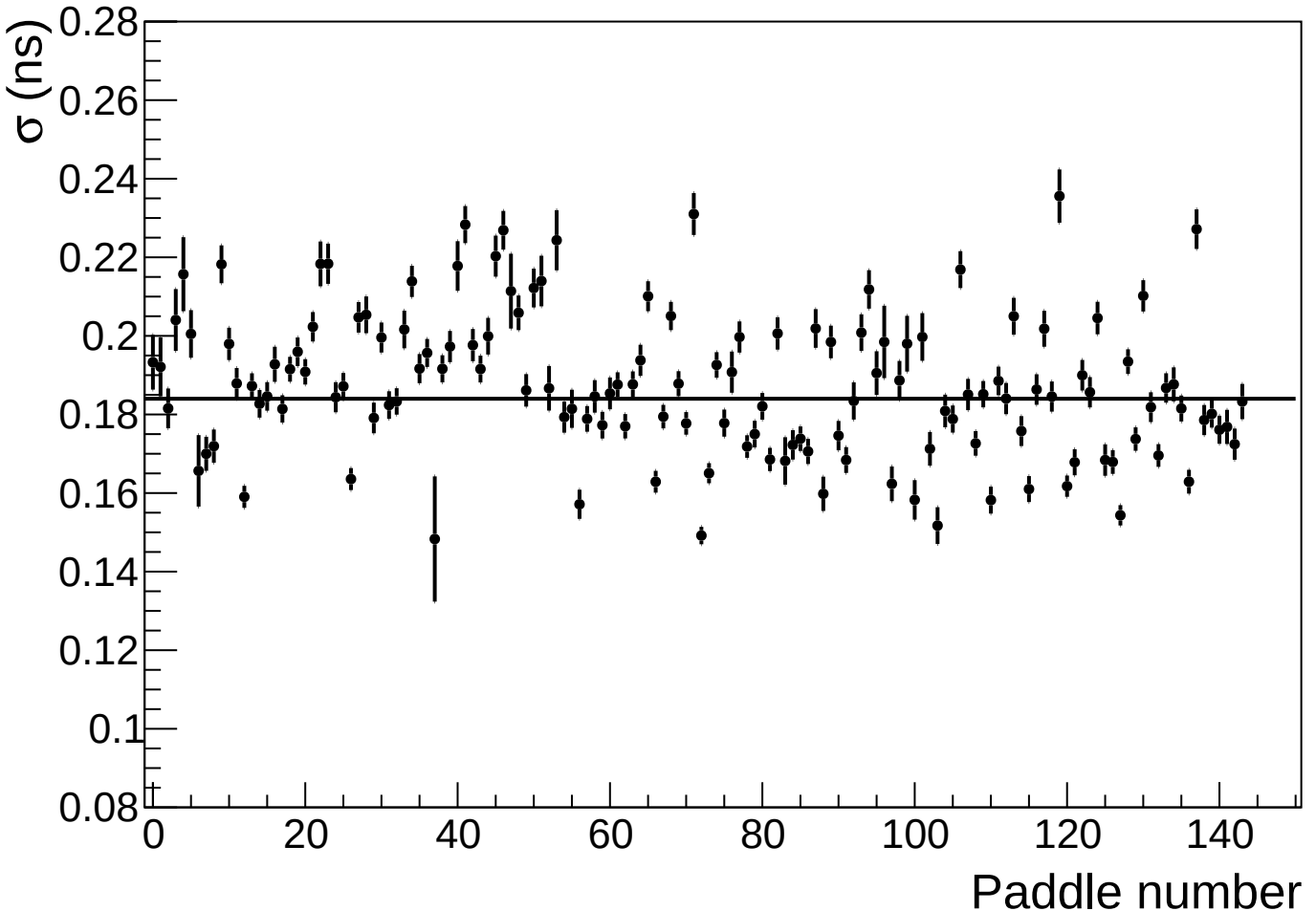
σ (ns)
0.28
0.26
0.24
0.22
0.2
0.18
0.16
0.14
0.12
0.1
0.08
0
20
40
60
80
100
120
140
Paddle number

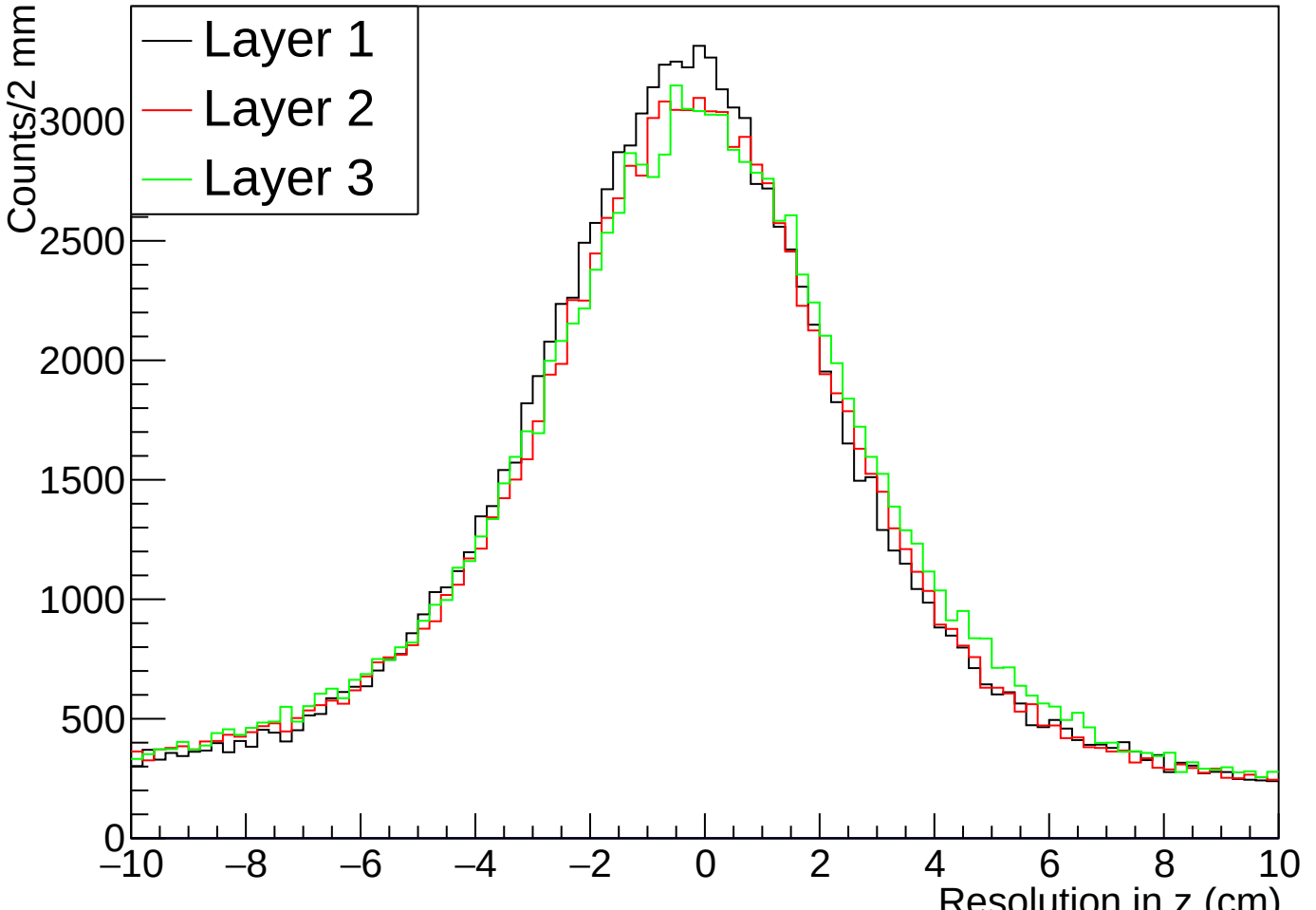
Layer 1
Layer 2
Layer 3
Counts/2 mm
3000
2500
2000
1500
1000
500
0
–10
–8
–6
–4
–2
0
2
4
6
8
10
Resolution in z (cm)

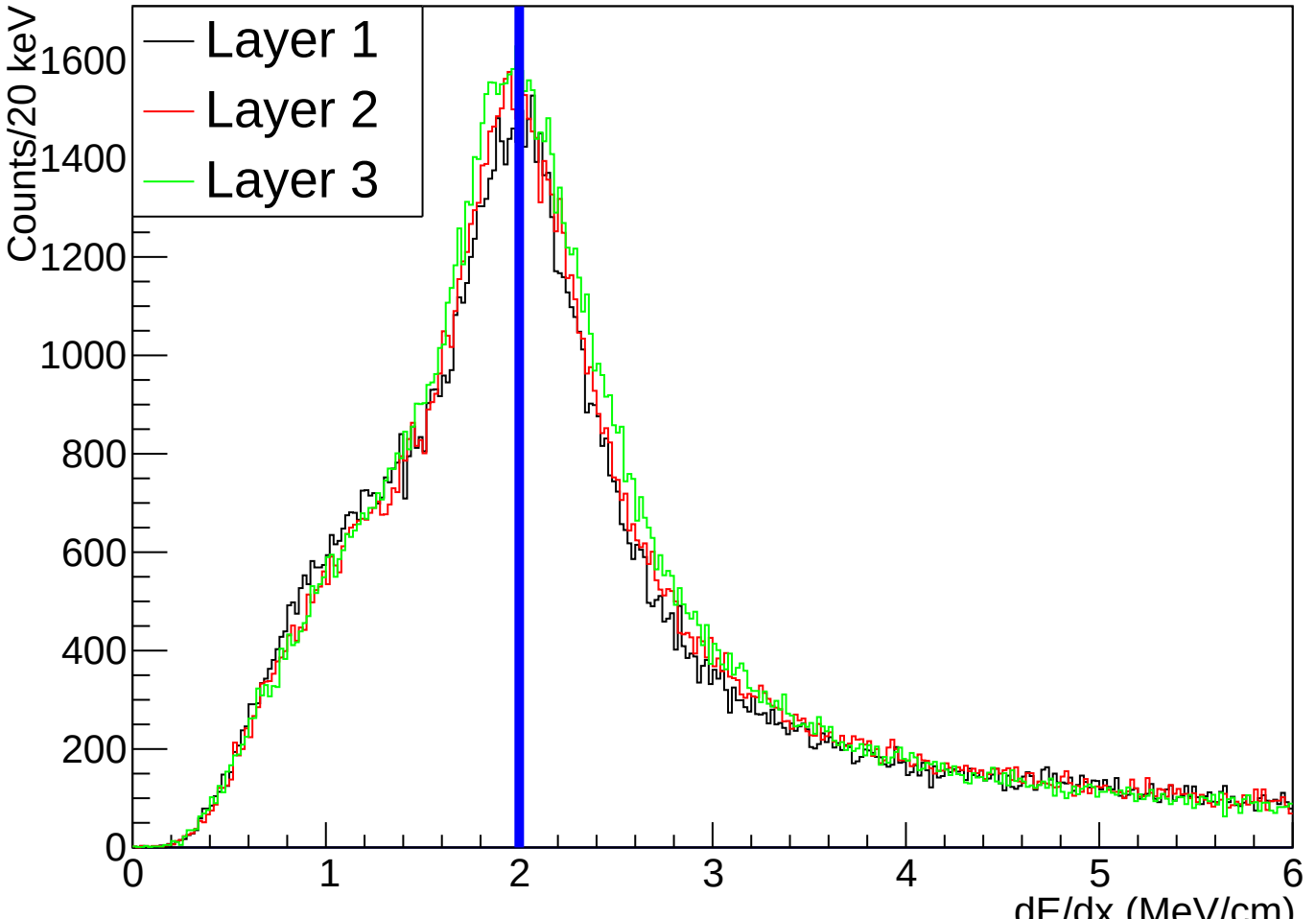
Layer 1
Layer 2
Layer 3
Counts/20 keV
1600
1400
1200
1000
800
600
400
200
0
0
1
2
3
4
5
6
dE/dx (MeV/cm)

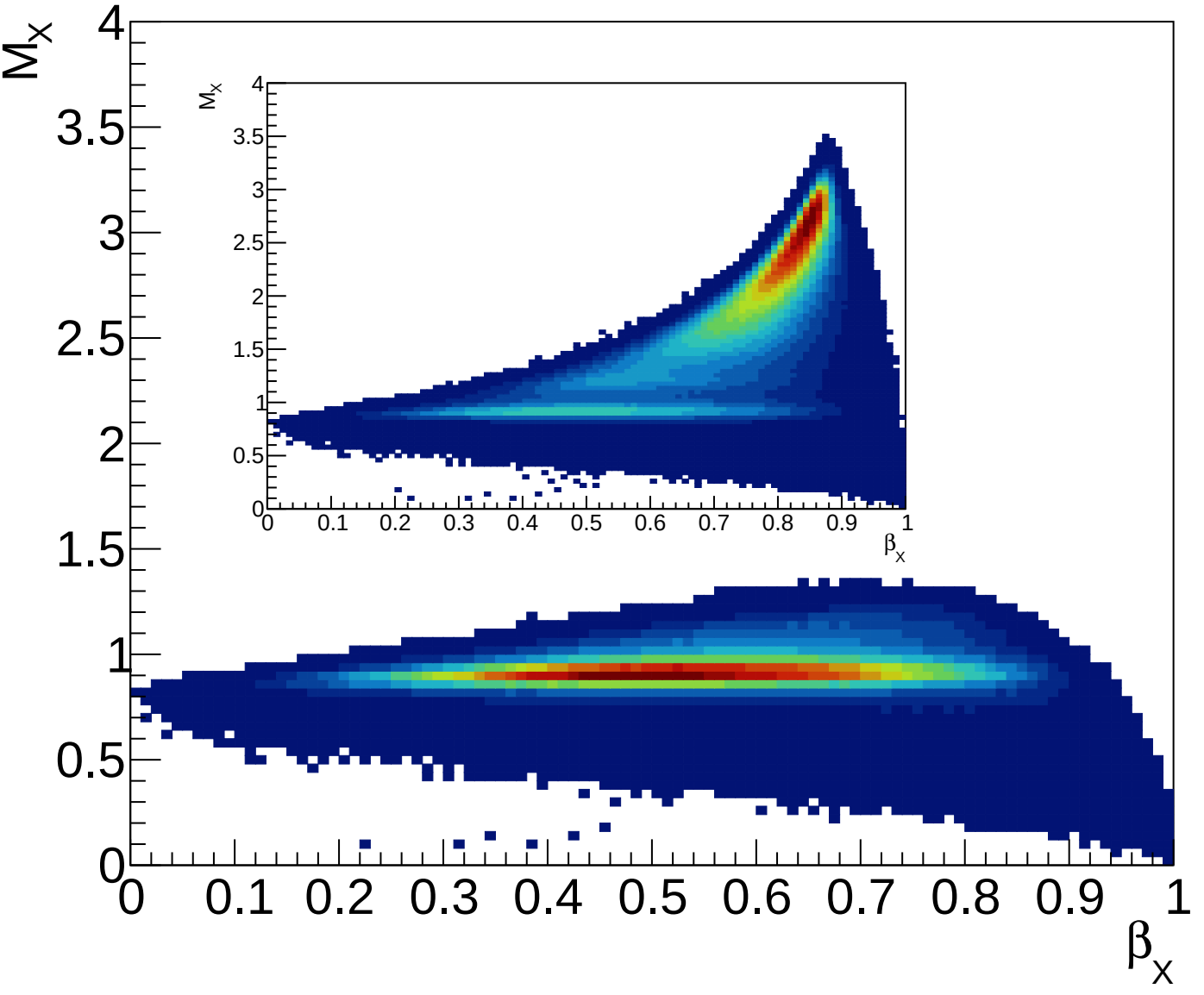
M_X
4
3.5
3
2.5
2
1.5
1
0.5
0
0 0.1 0.2 0.3 0.4 0.5 0.6 0.7 0.8 0.9 1
β_X
M_X
4
3.5
3
2.5
2
1.5
1
0.5
0
0 0.1 0.2 0.3 0.4 0.5 0.6 0.7 0.8 0.9 1
β_X

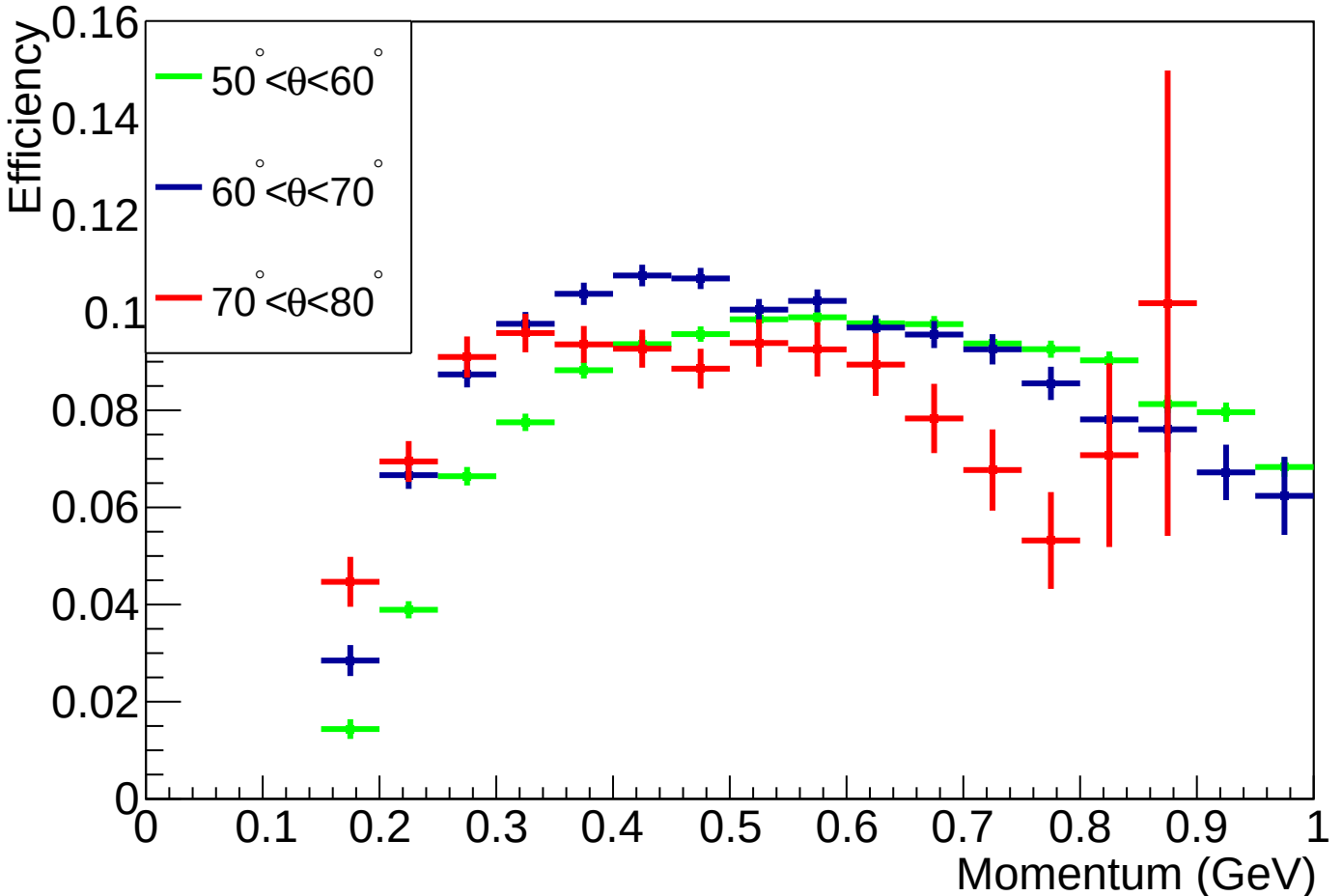
Efficiency
0.16
0.14
0.12
0.1
0.08
0.06
0.04
0.02
0
50°<θ<60°
60°<θ<70°
70°<θ<80°
0
0.1
0.2
0.3
0.4
0.5
0.6
0.7
0.8
0.9
1
Momentum (GeV)